

Measurements of CP violation in the three-body phase space of charmless B^\pm decays

R. Aaij *et al.**

(LHCb Collaboration)

(Received 25 August 2014; published 11 December 2014)

The charmless three-body decay modes $B^\pm \rightarrow K^\pm \pi^+ \pi^-$, $B^\pm \rightarrow K^\pm K^+ K^-$, $B^\pm \rightarrow \pi^\pm K^+ K^-$ and $B^\pm \rightarrow \pi^\pm \pi^+ \pi^-$ are reconstructed using data, corresponding to an integrated luminosity of 3.0 fb^{-1} , collected by the LHCb detector. The inclusive CP asymmetries of these modes are measured to be

$$A_{CP}(B^\pm \rightarrow K^\pm \pi^+ \pi^-) = +0.025 \pm 0.004 \pm 0.004 \pm 0.007,$$

$$A_{CP}(B^\pm \rightarrow K^\pm K^+ K^-) = -0.036 \pm 0.004 \pm 0.002 \pm 0.007,$$

$$A_{CP}(B^\pm \rightarrow \pi^\pm \pi^+ \pi^-) = +0.058 \pm 0.008 \pm 0.009 \pm 0.007,$$

$$A_{CP}(B^\pm \rightarrow \pi^\pm K^+ K^-) = -0.123 \pm 0.017 \pm 0.012 \pm 0.007,$$

where the first uncertainty is statistical, the second systematic, and the third is due to the CP asymmetry of the $B^\pm \rightarrow J/\psi K^\pm$ reference mode. The distributions of these asymmetries are also studied as functions of position in the Dalitz plot and suggest contributions from rescattering and resonance interference processes.

DOI: 10.1103/PhysRevD.90.112004

PACS numbers: 14.40.Nd, 11.30.Er, 11.30.Hv

I. INTRODUCTION

The violation of CP symmetry is well established experimentally in the quark sector and, in the Standard Model (SM), is explained by the Cabibbo-Kobayashi-Maskawa [1] matrix through the presence of a single irreducible complex phase. Although the SM is able to describe all CP asymmetries observed experimentally in particle decays, the amount of CP violation within the SM is insufficient to explain the matter-antimatter asymmetry of the Universe [2].

The decays of B mesons with three charged charmless mesons in the final state offer interesting opportunities to search for different sources of CP violation, through the study of the signature of these sources in the Dalitz plot. Several theoretical studies modeled the dynamics of the decays in terms of two-body intermediate states, such as

$\rho(770)K^\pm$ or $K^{*0}(892)\pi^\pm$ for $B^\pm \rightarrow K^\pm \pi^+ \pi^-$ decays, and $\phi(1020)K^\pm$ for $B^\pm \rightarrow K^\pm K^+ K^-$ decays (see e.g. Ref. [3]). These intermediate states were identified through amplitude analyses in which a resonant model was assumed. One method of performing such analyses was used by the Belle and the BABAR collaborations and significant CP violation was observed in the intermediate $\rho^0 K^\pm$ state [4,5] and in the ϕK^\pm channel [6]. No significant inclusive CP asymmetry

(integrated over the Dalitz plot) was found in $B^\pm \rightarrow K^\pm \pi^+ \pi^-$ or $B^\pm \rightarrow K^\pm K^+ K^-$ decays [4,6]. Another method is to measure the CP asymmetry in different regions of the three-body phase space. The LHCb Collaboration measured nonzero inclusive CP asymmetries and larger local asymmetries in the decays $B^\pm \rightarrow K^\pm \pi^+ \pi^-$, $B^\pm \rightarrow K^\pm K^+ K^-$ [7], $B^\pm \rightarrow \pi^\pm K^+ K^-$ and $B^\pm \rightarrow \pi^\pm \pi^+ \pi^-$ [8] using a sample corresponding to 1.0 fb^{-1} of data. These results suggested that final-state interactions may be a contributing factor to CP violation [9,10].

Direct CP violation requires the existence of amplitudes with differences in both their weak and their strong phases. The value of the weak phase can be accessed through interference between tree-level contributions to charmless B decays and other amplitudes (e.g. penguins). The strong phase can originate from three different sources in charmless three-body decays. The first source is related to short-distance processes where the gluon involved in the penguin contribution is timelike, i.e. the momentum transfer satisfies $q^2 > 4m_i^2$, where m_i represents the mass of either the u or the c quark present in the loop diagram [11]. This process is similar to that proposed for two-body decays where CP violation is caused by short-distance processes [12]. The remaining two sources are related to long-distance effects involving hadron-hadron interactions in the final state. Interference between intermediate states of the decay can introduce large strong-phase differences, and therefore induce local asymmetries in the phase space [9,13–16]. Another mechanism is final-state $KK \leftrightarrow \pi\pi$ rescattering, which can occur between decay channels having the same flavor quantum numbers [7–10]. Conservation of CPT symmetry constrains hadron

* Full author list given at the end of the article.

Published by the American Physical Society under the terms of the Creative Commons Attribution 3.0 License. Further distribution of this work must maintain attribution to the author(s) and the published articles title, journal citation, and DOI.

rescattering so that the sum of the partial decay widths of all channels with the same final-state quantum numbers related by the scattering matrix must equal that of their charge-conjugated decays [17]. The effects of SU(3) flavor symmetry breaking have also been investigated and can explain part of the pattern of CP violation reported by LHCb [9,17–19].

In this paper, the inclusive CP asymmetries of $B^\pm \rightarrow K^\pm \pi^+ \pi^-$, $B^\pm \rightarrow K^\pm K^+ K^-$, $B^\pm \rightarrow \pi^\pm K^+ K^-$ and $B^\pm \rightarrow \pi^\pm \pi^+ \pi^-$ decays (henceforth collectively referred to as $B^\pm \rightarrow h^\pm h^+ h^-$ decays) are measured, and local asymmetries in specific regions of the phase space are studied. All asymmetries are measured using the $B^\pm \rightarrow J/\psi K^\pm$ channel, which has similar topology and negligible CP violation, as a reference, thus allowing corrections to be made for production and instrumental asymmetries. We use a sample of proton-proton collisions collected in 2011 (2012) at a center-of-mass energy of 7(8) TeV and corresponding to an integrated luminosity of 1.0(2.0) fb⁻¹. This analysis supersedes that of Refs. [7,8], by using a larger data sample, improved particle identification and a more performant event selection.

II. LHCb DETECTOR AND DATA SET

The LHCb detector [20] is a single-arm forward spectrometer covering the pseudorapidity range $2 < \eta < 5$, designed for the study of particles containing b or c quarks. The detector includes a high-precision tracking system consisting of a silicon-strip vertex detector surrounding the pp interaction region, a large-area silicon-strip detector located upstream of a dipole magnet with a bending power of about 4 Tm, and three stations of silicon-strip detectors and straw drift tubes placed downstream. The tracking system provides a measurement of momentum, p , with a relative uncertainty that varies from 0.4% at low momentum to 0.6% at 100 GeV/ c . The minimum distance of a track to a primary vertex, the impact parameter, is measured with a resolution of $(15 + 29/p_T) \mu\text{m}$, where p_T is the component of p transverse to the beam, in GeV/ c . Charged hadrons are identified using two ring-imaging Cherenkov (RICH) detectors [21]. Photon, electron and hadron candidates are identified by a calorimeter system consisting of scintillating-pad and preshower detectors, an electromagnetic calorimeter and a hadronic calorimeter. Muons are identified by a system composed of alternating layers of iron and multiwire proportional chambers [22].

The trigger [23] consists of a hardware stage, based on information from the calorimeter and muon systems, followed by a software stage, which applies full event reconstruction. At the hardware trigger stage, events are required to have a muon with high p_T or a hadron, photon or electron with high transverse energy in the calorimeters. For hadrons, the transverse energy threshold is 3.5 GeV. In this analysis two partially overlapping categories of events

selected by the hardware trigger are considered: events where one of the hadrons from the B^\pm decay is used in the trigger decision (the “trigger on signal” sample), and events that are triggered by particles other than those hadrons from the B^\pm decay (the “trigger independent of signal” sample).

At the software trigger stage, events must have at least one good-quality track from the signal decay candidate with high p_T and a significant displacement from any primary vertex (PV). A secondary vertex, consisting of three good-quality tracks that have significant displacements from any PV, is also required.

The magnetic field polarity is reversed regularly during the data taking to reduce any potential bias from charged particle and antiparticle detection asymmetries. The magnetic field bends charged particles in the horizontal plane and the two polarities are referred to as “up” and “down.” The fraction of data collected with the magnet down polarity is approximately 60% in 2011, and 52% in 2012.

Possible residual charge-dependent asymmetries, which may originate from left-right differences in detection efficiency, are studied by comparing measurements from data with inverted magnet polarities and found to be negligible. Since the detection and production asymmetries are expected to change between 2011 and 2012 due to different data-taking conditions, the analysis is carried out separately for the 2011 and 2012 data and the results are combined.

The simulated events are generated using PYTHIA8 [24] with a specific LHCb configuration [25]. Decays of hadronic particles are produced by EVTGEN [26], in which final-state radiation is generated using PHOTOS [27]. The interaction of the generated particles with the detector and its response are implemented using the GEANT4 toolkit [28] as described in Ref. [29].

III. EVENT SELECTION

Since the four B^\pm signal decay modes considered are topologically and kinematically similar, the same selection criteria are used for each, except for the particle identification requirements, which are specific to each final state. The decay $B^\pm \rightarrow J/\psi K^\pm$, $J/\psi \rightarrow \mu^+ \mu^-$ serves as a control channel for $B^\pm \rightarrow h^\pm h^+ h^-$ decay modes. Since it has negligible CP violation, the raw asymmetry observed in $B^\pm \rightarrow J/\psi K^\pm$ decays is entirely due to production and detection asymmetries. The control channel has a similar topology to the signal and the sample passes the same trigger, kinematic, and kaon particle identification selection as the signal samples. The kaons from $B^\pm \rightarrow J/\psi K^\pm$ decays also have similar kinematic properties in the laboratory frame to those from the $B^\pm \rightarrow K^\pm \pi^+ \pi^-$ and $B^\pm \rightarrow K^\pm K^+ K^-$ modes.

In a preselection stage, loose requirements are imposed on the p , p_T and the displacement from any PV for the tracks, and on the distance of closest approach between each pair of tracks. The three tracks must form a

good-quality secondary vertex that has a significant separation from its associated PV. The momentum vector of the reconstructed B^\pm candidate has to point back to the PV.

Charm-meson contributions are removed by excluding events where two-body invariant masses $m(\pi^+\pi^-)$, $m(K^\pm\pi^\mp)$ and $m(K^+K^-)$ are within 30 MeV/ c^2 of the known value of the D^0 mass [30]. The contribution of misidentified $B^\pm \rightarrow J/\psi K^\pm$ decays is also excluded from the $B^\pm \rightarrow K^\pm\pi^+\pi^-$ sample by removing the mass region $3.05 < m(\pi^+\pi^-) < 3.15$ GeV/ c^2 .

A multivariate selection based on a boosted decision tree (BDT) algorithm [31–33] is applied to reduce the combinatorial background. The input variables, which are a subset of those used in the preselection, are common to all four decay modes. The BDT is trained using a mixture of simulated signal events as the signal sample, and events reconstructed as $B^\pm \rightarrow \pi^\pm\pi^+\pi^-$ decays with $5.40 < m(\pi^+\pi^+\pi^-) < 5.58$ GeV/ c^2 as the background sample. The requirement on the BDT response is chosen to maximize the ratio $N_S/\sqrt{N_S + N_B}$, where N_S and N_B represent the expected number of signal and background candidates, respectively, within an invariant mass window of approximately 40 MeV/ c^2 around the signal peak. Since the optimal requirements are similar for the different channels, the same BDT response requirement is chosen for all channels, to simplify the evaluation of the systematic uncertainties. The BDT selection improves the efficiencies for selecting signal events by approximately 50%, compared to the cut-based selection used in Refs. [7] and [8].

Particle identification is used to reduce the cross-feed from other B decays in which hadrons are incorrectly classified. The main source is $K \rightarrow \pi$ and $\pi \rightarrow K$ misidentification, while $p \rightarrow K$ and $p \rightarrow \pi$ misidentification is negligible. Muons are rejected by a veto applied to each track [34]. After the full selection, events with more than one candidate in the range $4.8 < m(B) < 5.8$ GeV/ c^2 are discarded. This removes approximately 1–2% of candidates.

The $B^\pm \rightarrow J/\psi K^\pm$ control channel is selected using the same criteria as described above, with two exceptions that enhance the selection of J/ψ mesons decaying to two muons: criteria used to identify charged pions are removed and the requirement $3.05 < m(\pi^+\pi^-) < 3.15$ GeV/ c^2 is applied.

IV. DETERMINATION OF SIGNAL YIELDS

For each channel the yields and raw asymmetry are extracted from a single simultaneous unbinned extended maximum-likelihood fit to the B^+ and B^- invariant mass distribution. The signal components of all four channels are parametrized by a Gaussian function with widths and tails that differ either side of the peak to account for asymmetric effects such as final-state radiation. The means and widths are allowed to vary in the fits, while the tail parameters are

fixed to values obtained from simulation. The combinatorial backgrounds are described by exponential functions. The backgrounds due to partially reconstructed four-body B decays are parametrized by an ARGUS function [35] convolved with a Gaussian function. The shapes and yields of peaking backgrounds, i.e. fully reconstructed B decays with at least one misidentified particle in the final state, are obtained from simulation of the relevant decay modes and fixed in the fits. The yields of the peaking and partially reconstructed background components are constrained to be equal for B^+ and B^- decays.

The invariant mass spectra of the four decay modes are shown in Fig. 1. The figure is illustrative only, as the asymmetries are obtained from separate fits of the samples divided by year, trigger selection and magnet polarity, and then combined as described in Sec. V.

The signal yields obtained for the combined 2011 and 2012 data samples are shown in Table I. The data samples are larger than those presented in Refs. [7] and [8] due to both an increase in the integrated luminosity and the use of a more efficient selection.

V. INCLUSIVE CP ASYMMETRY MEASUREMENT

The CP asymmetry of B^\pm decays to a final state f^\pm is defined as

$$A_{CP} \equiv \frac{\Gamma[B^- \rightarrow f^-] - \Gamma[B^+ \rightarrow f^+]}{\Gamma[B^- \rightarrow f^-] + \Gamma[B^+ \rightarrow f^+]}, \quad (1)$$

where Γ is the partial decay width. To determine the inclusive CP asymmetries, the raw asymmetries measured from the fits are corrected for effects induced by the detector efficiency, interactions of final-state particles with matter, and any asymmetry in the forward production rates between B^+ and B^- mesons. The raw asymmetry, A_{raw} , is written in terms of the B^- and B^+ event yields as

$$A_{\text{raw}} \equiv \frac{N_{B^-} - N_{B^+}}{N_{B^-} + N_{B^+}}, \quad (2)$$

where the numbers of signal events N_{B^-} and N_{B^+} are related to the asymmetries by

$$\begin{aligned} N_{B^-} &= (1 + A_{CP} + A_D + A_P) \frac{N_S}{2} \times \frac{\langle \epsilon^+ \rangle}{\langle \epsilon^- \rangle}, \\ N_{B^+} &= (1 - A_{CP} - A_D - A_P) \frac{N_S}{2}. \end{aligned} \quad (3)$$

Here, A_P is the B^\pm -meson production asymmetry, N_S are the total yields, and $\langle \epsilon^\pm \rangle$ are the average efficiencies for selecting and reconstructing B^+ and B^- decays, respectively. The efficiency is computed on an event-by-event basis and depends on the position in the Dalitz plot. The term A_D accounts for residual detection asymmetries, such as differences in interactions of final-state particles with the

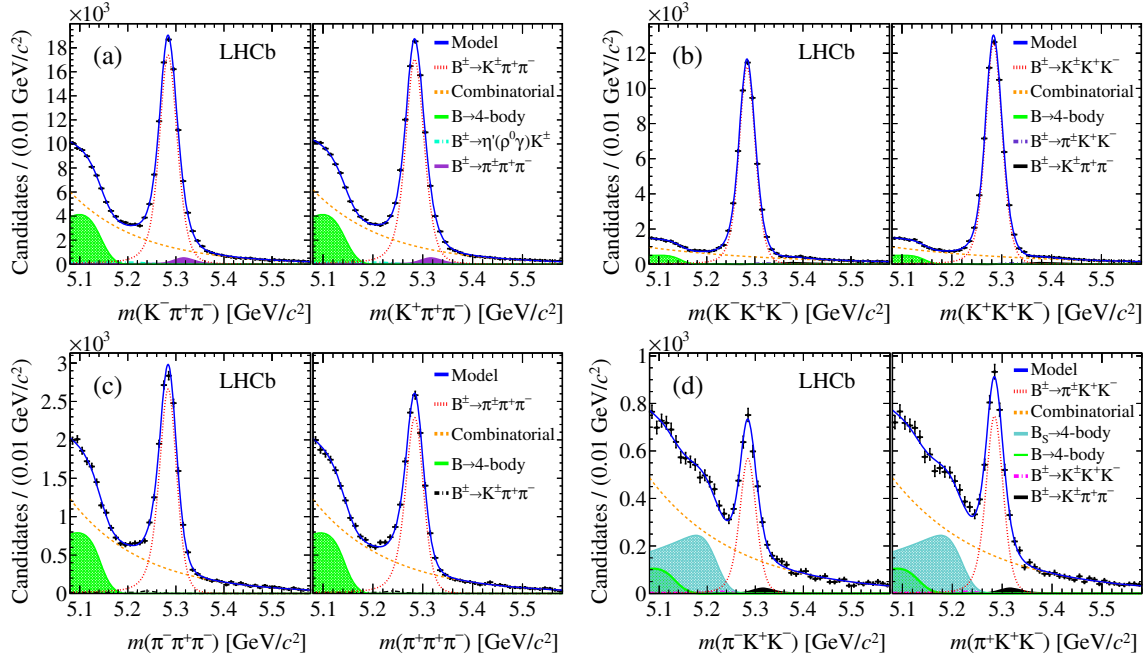


FIG. 1 (color online). Invariant mass spectra of (a) $B^\pm \rightarrow K^\pm \pi^+ \pi^-$, (b) $B^\pm \rightarrow K^\pm K^+ K^-$, (c) $B^\pm \rightarrow \pi^\pm \pi^+ \pi^-$ and (d) $B^\pm \rightarrow \pi^\pm K^+ K^-$ decays. The left panel in each figure shows the B^- candidates and the right panel shows the B^+ candidates. The results of the unbinned maximum-likelihood fits are overlaid. The main components of the fits are also shown.

detector material or left-right asymmetries that may not be properly represented in the Monte Carlo.

The three final-state hadrons are treated as the combination of a pair of same-flavor, charge-conjugate hadrons $h^+ h^- = \pi^+ \pi^-, K^+ K^-$, and an unpaired hadron h'^{\pm} with the same charge as the B^\pm meson. The detection asymmetry $A_D^{h'}$ is given in terms of the charge-conjugate detection efficiencies of the unpaired hadron h'^{\pm} , and the production asymmetry A_P is given in terms of the B^\pm production rates.

The raw asymmetry is expressed in terms of A_{CP} , A_P and $A_D^{h'}$ using Eqs. (2) and (3),

$$A_{\text{raw}} = \frac{A_{CP} + A_P + A_D^{h'} + A_{CP} A_P A_D^{h'}}{1 + A_{CP} A_P + A_{CP} A_D^{h'} + A_P A_D^{h'}}. \quad (4)$$

For small asymmetries the products are negligible, and the raw asymmetry becomes

$$A_{\text{raw}} \approx A_{CP} + A_P + A_D^{h'}. \quad (5)$$

TABLE I. Signal yields of charmless three-body B^\pm decays for the full data set.

| Decay mode | Yield |
|---|------------------|
| $B^\pm \rightarrow K^\pm \pi^+ \pi^-$ | 181074 ± 556 |
| $B^\pm \rightarrow K^\pm K^+ K^-$ | 109240 ± 354 |
| $B^\pm \rightarrow \pi^\pm \pi^+ \pi^-$ | 24907 ± 222 |
| $B^\pm \rightarrow \pi^\pm K^+ K^-$ | 6161 ± 172 |

Throughout this paper, Eq. (5) is used in calculating the inclusive asymmetries, as all terms are sufficiently small. For the determination of the asymmetries in regions of the phase space where the raw asymmetries are large, the full formula of Eq. (4) is applied.

The four decay channels are divided into two categories according to the flavor of the final-state hadron h'^{\pm} . For the $B^\pm \rightarrow K^\pm \pi^+ \pi^-$ and $B^\pm \rightarrow K^\pm K^+ K^-$ decay channels, the CP asymmetry is expressed in terms of the raw asymmetry and correction terms given by the sum of the B^\pm production asymmetry and the kaon detection asymmetry, A_P and A_D^K . For the $B^\pm \rightarrow \pi^\pm K^+ K^-$ and $B^\pm \rightarrow \pi^\pm \pi^+ \pi^-$ decay channels, the pion detection asymmetry A_D^π is used. The CP asymmetries are calculated as

$$\begin{aligned} A_{CP}(Khh) &= A_{\text{raw}}(hhK) - A_P - A_D^K = A_{\text{raw}}(hhK) - A_\Delta, \\ A_{CP}(\pi hh) &= A_{\text{raw}}(hh\pi) - A_P - A_D^\pi = A_{\text{raw}}(hh\pi) \\ &\quad - A_\Delta + A_D^K - A_D^\pi. \end{aligned} \quad (6)$$

The correction term A_Δ is measured using approximately 265 000 $B^\pm \rightarrow J/\psi(\mu^+ \mu^-) K^\pm$ decays. The correction is obtained from the raw asymmetry of the $B^\pm \rightarrow J/\psi K^\pm$ mode as

$$A_\Delta = A_{\text{raw}}(J/\psi K^\pm) - A_{CP}(J/\psi K^\pm), \quad (7)$$

using the world average of the CP asymmetry $A_{CP}(J/\psi K^\pm) = (0.1 \pm 0.7)\%$ [30].

The pion detection asymmetry, $A_D^\pi = (0.00 \pm 0.25)\%$, has been previously measured by LHCb [36] and is consistent with being independent of p and p_T . The production asymmetry is obtained from the same sample of $B^\pm \rightarrow J/\psi K^\pm$ decays as $A_P = A_\Delta - A_D^K$, and is consistent with being constant in the interval of momentum measured. Here the kaon interaction asymmetry $A_D^K = (-1.26 \pm 0.18)\%$ is measured in a sample of $D^{*+} \rightarrow \pi^+ D^0 \rightarrow \pi^+ K^- \pi^+ \pi^- \pi^+$ decays, where the D^{*+} is produced in the decay of a B meson. The value of A_D^K is obtained by measuring the ratio of fully to partially reconstructed D^{*+} decays [36].

Since neither the detector efficiencies nor the observed raw asymmetries are uniform across the Dalitz plot, an acceptance correction is applied to the integrated raw asymmetries. This is determined by the ratio of the B^- and B^+ average efficiencies in simulated events, reweighted to reproduce the population of signal data in bins of the Dalitz plot. In addition, to account for the small charge asymmetry introduced by the hadronic hardware trigger, the data are divided into the trigger independent of signal and the trigger on signal samples, as discussed in Sec. II. The CP asymmetries are calculated using Eqs. (6) and (7), applied to the acceptance-corrected raw asymmetries of the samples collected in each trigger configuration. The inclusive CP asymmetry of each mode is the weighted average of the CP asymmetries for the samples divided by trigger and year of data taking, taking into account the correlation between trigger samples as described in Ref. [37].

VI. SYSTEMATIC UNCERTAINTIES

AND RESULTS

Several sources of systematic uncertainty are considered. These include potential mismodelings in the mass fits, the phase-space acceptance corrections and the trigger composition of the samples.

The systematic uncertainties due to the mass fit models are evaluated as the full difference in CP asymmetry resulting from variations of the model. The alternative fits have good quality and describe the data accurately. To estimate the uncertainty due to the choice of the signal mass function, the initial model is replaced by an alternative empirical distribution [38]. A systematic uncertainty to account for the use of equal means and widths for B^- and B^+ signal peaks in the default fit is assigned by repeating the fits with these parameters allowed to vary independently. The resulting means and widths are found to agree and the difference in the value of A_{CP} is assigned as a systematic uncertainty.

The systematic uncertainty associated with the peaking background fractions reflects the uncertainties in the expected yields determined from simulation, and the

influence of combining 2011 and 2012 simulated samples when determining the fractions in the nominal fit, by repeating the fits with the background fractions obtained for the samples separately. The uncertainty due to background shape is obtained by increasing the width of the Gaussian function according to the observed differences between simulation and data for peaking backgrounds, and allowing the four-body shape to vary in the fit. Similarly, the possibility of nonzero background asymmetries is tested by letting the peaking and four-body-background normalizations vary separately for B^- and B^+ fits. The signal model variations and the background asymmetry are the dominant systematic uncertainties related to the fit procedure.

The systematic uncertainty related to the acceptance correction procedure consists of two parts: the statistical uncertainty on the detection efficiency due to the finite size of the simulated samples, and the uncertainty due to the choice of binning, which is evaluated by varying the binning used in the efficiency correction.

A study is performed to investigate the effect of having different trigger admixtures in the signal and the control channels. The acceptance-corrected CP asymmetries are measured separately for each trigger category and found to agree, and therefore no additional systematic uncertainty is assigned. Performing this comparison validates the assumption that the detection asymmetry factorizes between the h^+h^- pair and the h'^\pm , within the statistical precision of the test.

The systematic uncertainties, separated by year, are shown in Table II, where the total systematic uncertainty is the sum in quadrature of the individual contributions. The uncertainties on A_D^π and A_D^K are only considered as systematic uncertainties for $B^\pm \rightarrow \pi^\pm \pi^+ \pi^-$ and $B^\pm \rightarrow \pi^\pm K^+ K^-$ decays, following Eq. (6). The systematic uncertainty of the 2011 and 2012 combination is taken to be the greater of these two values.

The results for the integrated CP asymmetries are

$$\begin{aligned} A_{CP}(B^\pm \rightarrow K^\pm \pi^+ \pi^-) &= +0.025 \pm 0.004 \pm 0.004 \pm 0.007, \\ A_{CP}(B^\pm \rightarrow K^\pm K^+ K^-) &= -0.036 \pm 0.004 \pm 0.002 \pm 0.007, \\ A_{CP}(B^\pm \rightarrow \pi^\pm \pi^+ \pi^-) &= +0.058 \pm 0.008 \pm 0.009 \pm 0.007, \\ A_{CP}(B^\pm \rightarrow \pi^\pm K^+ K^-) &= -0.123 \pm 0.017 \pm 0.012 \pm 0.007, \end{aligned}$$

where the first uncertainty is statistical, the second systematic, and the third is due to the limited knowledge of the CP asymmetry of the $B^\pm \rightarrow J/\psi K^\pm$ reference mode [30]. The significances of the inclusive charge asymmetries, calculated by dividing the central values by the sum in quadrature of the uncertainties, are 2.8 standard deviations (σ) for $B^\pm \rightarrow K^\pm \pi^+ \pi^-$ decays, 4.3 σ for $B^\pm \rightarrow K^\pm K^+ K^-$ decays, 4.2 σ for $B^\pm \rightarrow \pi^\pm \pi^+ \pi^-$ decays and 5.6 σ for $B^\pm \rightarrow \pi^\pm K^+ K^-$ decays.

TABLE II. Systematic uncertainties on the measured asymmetries, where the total is the sum in quadrature of the individual contributions. The A_D^π uncertainty is taken from Ref. [36].

| Systematic uncertainty | $A_{CP}(K\pi\pi)$ | | $A_{CP}(KKK)$ | | $A_{CP}(\pi\pi\pi)$ | | $A_{CP}(\pi KK)$ | |
|------------------------|-------------------|--------|---------------|--------|---------------------|--------|------------------|--------|
| | 2011 | 2012 | 2011 | 2012 | 2011 | 2012 | 2011 | 2012 |
| Signal model | | | | | | | | |
| Function | 0.0000 | 0.0001 | 0.0002 | 0.0005 | 0.0046 | 0.0025 | 0.0028 | 0.0046 |
| B^\pm parameters | 0.0006 | 0.0006 | 0.0005 | 0.0005 | 0.0032 | 0.0032 | 0.0027 | 0.0027 |
| Background | | | | | | | | |
| Fractions | 0.0000 | 0.0001 | 0.0002 | 0.0001 | 0.0001 | 0.0001 | 0.0010 | 0.0014 |
| Resolution | 0.0000 | 0.0001 | 0.0001 | 0.0000 | 0.0001 | 0.0000 | 0.0001 | 0.0004 |
| Asymmetry | 0.0031 | 0.0032 | 0.0015 | 0.0011 | 0.0017 | 0.0027 | 0.0011 | 0.0019 |
| Acceptance corr. | 0.0012 | 0.0018 | 0.0013 | 0.0013 | 0.0063 | 0.0051 | 0.0099 | 0.0092 |
| A_D^K uncertainty | ... | ... | ... | ... | 0.0018 | 0.0018 | 0.0018 | 0.0018 |
| A_D^π uncertainty | ... | ... | ... | ... | 0.0025 | 0.0025 | 0.0025 | 0.0025 |
| Total | 0.0034 | 0.0038 | 0.0020 | 0.0019 | 0.0090 | 0.0075 | 0.0113 | 0.0115 |

VII. CP ASYMMETRY IN THE PHASE SPACE

The Dalitz plot distributions in the signal region for the four channels are shown in Fig. 2. For the $B^\pm \rightarrow K^\pm K^+ K^-$ and $B^\pm \rightarrow \pi^\pm \pi^+ \pi^-$ decays, folded Dalitz plots are used. For a given event, the vertical axis of the Dalitz plot corresponds to the invariant mass squared of the decay with the highest value [$m^2(h^+h^-)_{\text{high}}$], while the horizontal axis is the invariant mass squared with the lowest value between the two [$m^2(h^+h^-)_{\text{low}}$].

The signal region is defined as the three-body invariant mass region within 34 MeV/ c^2 of the fitted mass, except

for the $B^\pm \rightarrow \pi^\pm K^+ K^-$ channel, for which the mass window is restricted to ± 17 MeV/ c^2 of the peak due to the larger background. The expected background contribution is not subtracted from the data presented in these figures. To improve the resolution, the Dalitz variables are calculated after refitting the candidates with their invariant masses constrained to the known B^\pm value [30]. The events are concentrated in low-mass regions, as expected for charmless decays dominated by resonant contributions.

In the $B^\pm \rightarrow K^\pm K^+ K^-$ decays, the region of $m^2(K^+K^-)_{\text{low}}$ around 1.0 GeV $^2/c^4$ corresponds to the

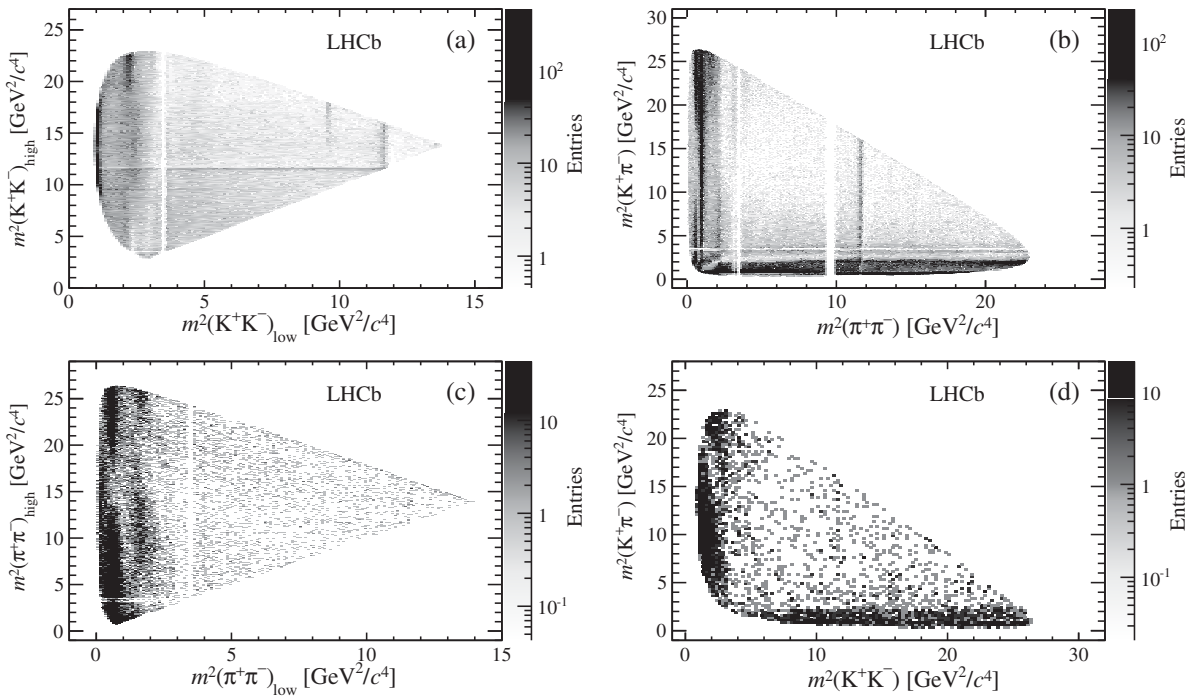


FIG. 2. Dalitz plot distributions of (a) $B^\pm \rightarrow K^\pm K^+ K^-$, (b) $B^\pm \rightarrow K^\pm \pi^+ \pi^-$, (c) $B^\pm \rightarrow \pi^\pm \pi^+ \pi^-$ and (d) $B^\pm \rightarrow \pi^\pm K^+ K^-$ candidates. The visible gaps correspond to the exclusion of the J/ψ (in the $B^\pm \rightarrow K^\pm \pi^+ \pi^-$ decay) and D^0 (all plots, except for the $B^\pm \rightarrow \pi^\pm K^+ K^-$ decay) mesons from the samples.

$\phi(1020)$ resonance, and that around $11.5 \text{ GeV}^2/c^4$ to the $\chi_{c0}(1P)$ meson. In the region $2\text{--}3 \text{ GeV}^2/c^4$, there are clusters that could correspond to the $f_2'(1525)$ or the $f_0(1500)$ resonances observed by *BABAR* in this decay mode [6]. The contribution of $B^\pm \rightarrow J/\psi K^\pm$ decays with $J/\psi \rightarrow K^+ K^-$ is visible around $9.6 \text{ GeV}^2/c^4$ in $m^2(K^+ K^-)$.

In the $B^\pm \rightarrow K^\pm \pi^+ \pi^-$ Dalitz plot, there are low-mass resonances in both $K^\pm \pi^\mp$ and $\pi^+ \pi^-$ spectra: $K^{*0}(892)$, $\rho^0(770)$, $f_0(980)$ and $K_{0,2}^{*0}(1430)$. In addition, the $\chi_{c0}(1P)$ resonance is seen at $m^2(\pi^+ \pi^-) \approx 11 \text{ GeV}^2/c^4$.

For $B^\pm \rightarrow \pi^\pm \pi^+ \pi^-$ decays, the resonances are the $\rho^0(770)$ at $m^2(\pi^+ \pi^-)_{\text{low}} < 1 \text{ GeV}^2/c^4$. In the region of $1.5 < m^2(\pi^+ \pi^-)_{\text{low}} < 2 \text{ GeV}^2/c^4$, there are clusters that could correspond to the $\rho^0(1450)$, the $f_2(1270)$ and the $f_0(1370)$ resonances observed by *BABAR* in this decay mode [39].

For $B^\pm \rightarrow \pi^\pm K^+ K^-$ decays, there is a cluster of events at $m^2(K^\pm \pi^\mp) < 2 \text{ GeV}^2/c^4$, which could correspond to the $K^{*0}(892)$ and $K_{0,2}^{*0}(1430)$ resonances. The $B^\pm \rightarrow \pi^\pm K^+ K^-$ decays are not expected to have a contribution from the $\phi(1020)$ resonance [40] and indeed, the $\phi(1020)$ contribution is not immediately apparent in the region of $m^2(K^+ K^-)$ around $1 \text{ GeV}^2/c^4$.

An inspection of the distribution of candidates from the B^+ mass sidebands confirms that the background is not

uniformly distributed, with combinatorial background events tending to be concentrated at the corners of the phase space, as these are dominated by low-momentum particles.

In addition to the inclusive charge asymmetries, the asymmetries are studied in bins of the Dalitz plots. Figure 3 shows these asymmetries, $A_{\text{raw}}^N \equiv \frac{N^- - N^+}{N^- + N^+}$, where N^- and N^+ are the background-subtracted, efficiency-corrected signal yields for B^- and B^+ decays, respectively. Background subtraction is done via a statistical tool to unfold data distributions called the *sPlot* technique [41] using the B^\pm candidate invariant mass as the discriminating variable. The binning is chosen adaptively, to allow approximately equal populations of the total number of entries ($N^- + N^+$) in each bin.

The A_{raw}^N distributions in the Dalitz plots reveal rich structures, which are more evident in the two-body invariant-mass projection plots. These are shown in Figs. 4 and 5 for the region of the ρ resonance in $B^\pm \rightarrow \pi^\pm \pi^+ \pi^-$ and $B^\pm \rightarrow K^\pm \pi^+ \pi^-$ decays, respectively. The projections are split according to the sign of $\cos \theta$, where θ is the angle between the momenta of the unpaired hadron and the resonance decay product with the same-sign charge. Figure 6 shows the projection onto the low $K^+ K^-$ invariant mass for the $B^\pm \rightarrow K^\pm K^+ K^-$ channel, while Fig. 7 shows the projection onto $m(K^+ K^-)$ for the $B^\pm \rightarrow \pi^\pm K^+ K^-$ mode.

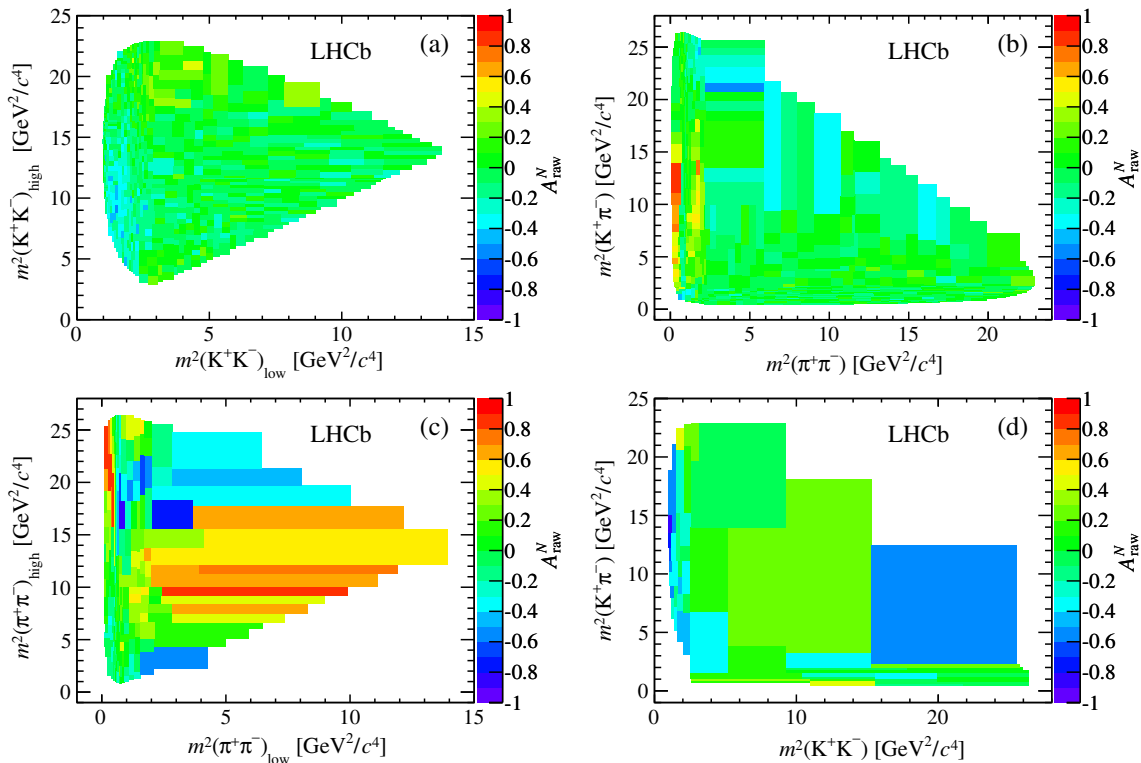


FIG. 3 (color online). Measured A_{raw}^N in Dalitz plot bins of background-subtracted and acceptance-corrected events for (a) $B^\pm \rightarrow K^\pm K^+ K^-$, (b) $B^\pm \rightarrow K^\pm \pi^+ \pi^-$, (c) $B^\pm \rightarrow \pi^\pm \pi^+ \pi^-$ and (d) $B^\pm \rightarrow \pi^\pm K^+ K^-$ decays.

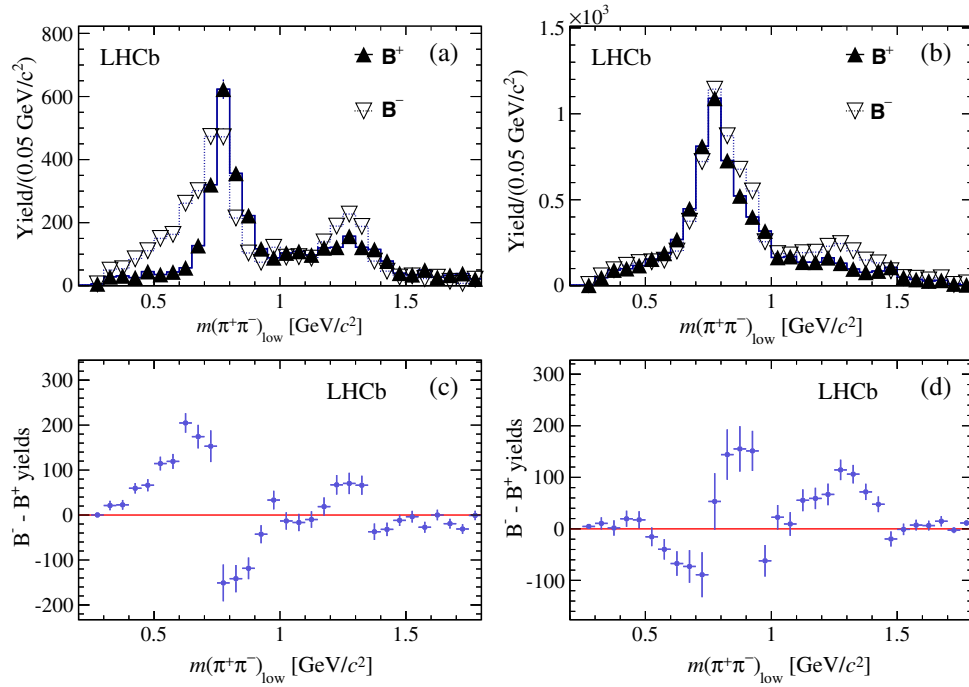


FIG. 4 (color online). Projections in bins of the $m(\pi^+\pi^-)_{\text{low}}$ variable of (a), (b) the number of B^- and B^+ signal events and (c), (d) their difference for $B^\pm \rightarrow \pi^\pm \pi^+ \pi^-$ decays. The plots are restricted to events with (a), (c) $\cos \theta < 0$ and (b), (d) $\cos \theta > 0$, with $\cos \theta$ defined in the text. The yields are acceptance-corrected and background-subtracted. A guide line for zero (horizontal red line) was included in plots (c) and (d).

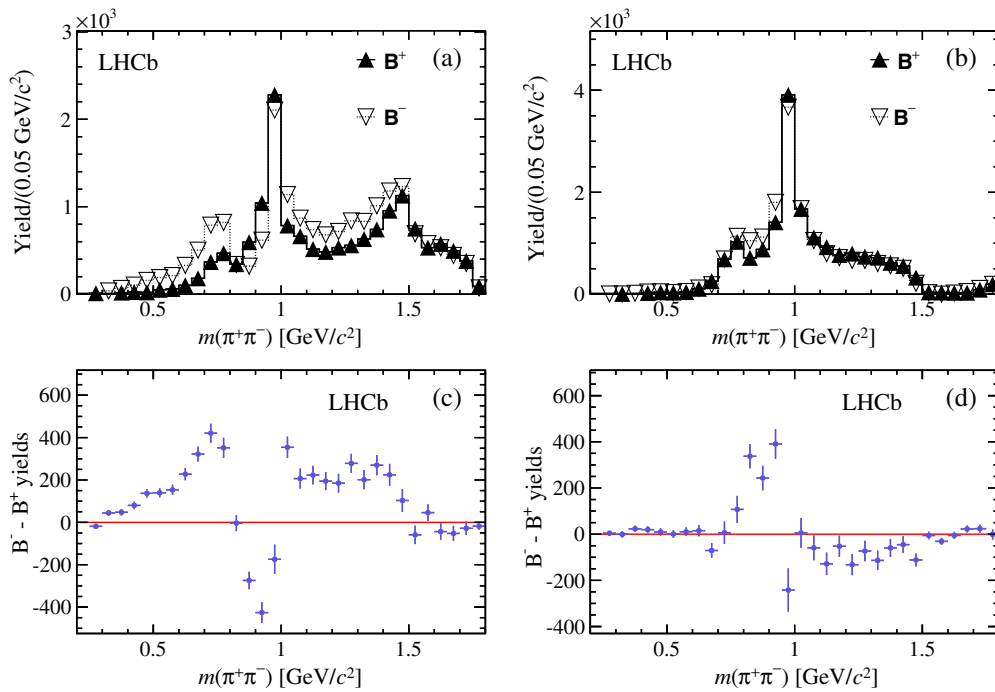


FIG. 5 (color online). Projections in bins of the $m(\pi^+\pi^-)$ variable of (a), (b) the number of B^- and B^+ signal events and (c), (d) their difference for $B^\pm \rightarrow K^\pm \pi^+ \pi^-$ decays. The plots are restricted to events with (a), (c) $\cos \theta < 0$ and (b), (d) $\cos \theta > 0$. The yields are acceptance-corrected and background-subtracted. A guide line for zero (horizontal red line) was included in plots (c) and (d).

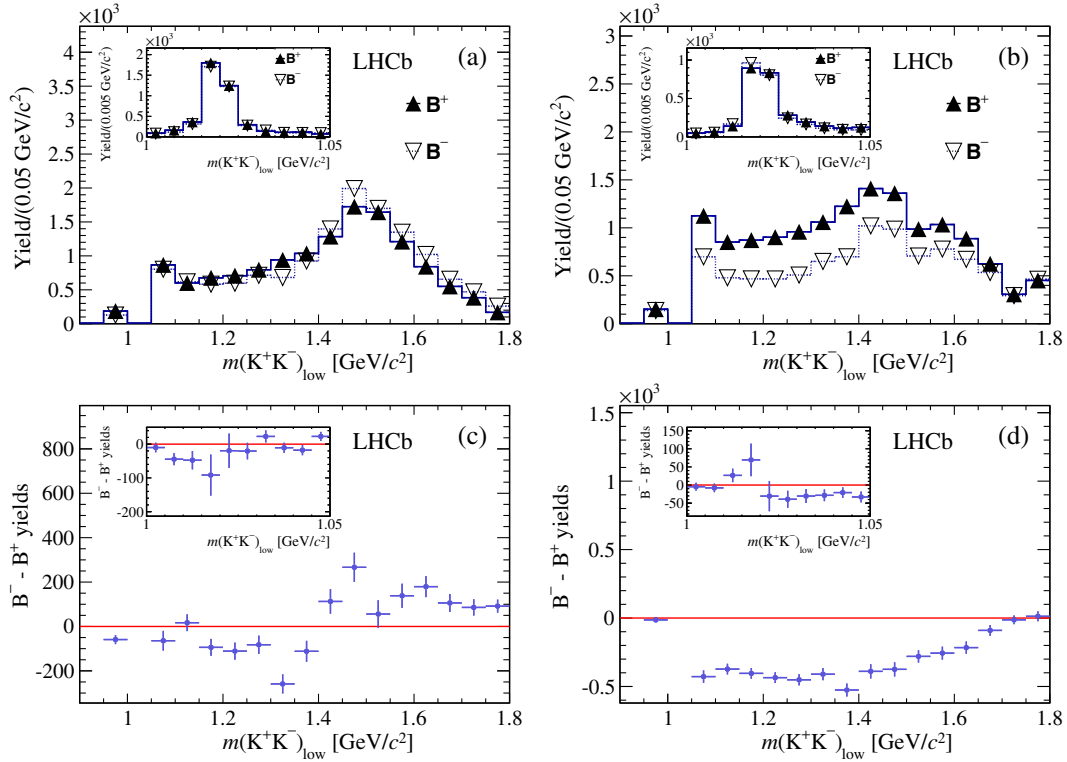


FIG. 6 (color online). Projections in bins of the $m(K^+K^-)_{\text{low}}$ variable of (a), (b) the number of B^- and B^+ signal events and (c), (d) their difference for $B^\pm \rightarrow K^\pm K^+ K^-$ decays. The inset plots show the ϕ resonance region of $m(K^+K^-)_{\text{low}}$ between 1.00 and 1.05 GeV/c^2 , which is excluded from the main plots. The plots are restricted to events with (a), (c) $\cos \theta < 0$ and (b), (d) $\cos \theta > 0$. The yields are acceptance-corrected and background-subtracted. A guide line for zero (horizontal red line) was included in plots (c) and (d).

The dynamic origin of the CP asymmetries seen in Fig. 3 can only be fully understood with an amplitude analysis of these channels. Nevertheless, the projections presented in Figs. 4, 5, 6 and 7 indicate two different sources of CP violation. The first one may be associated with the $\pi^+\pi^- \leftrightarrow K^+K^-$ rescattering strong-phase difference in the region around 1.0 to 1.5 GeV/c^2 [7,8]. In this region, there are more B^- than B^+ decays into final states including a $\pi^+\pi^-$ pair (positive CP asymmetry) and more B^+ than B^- into final states that include a K^+K^- pair (negative CP asymmetry). The second source of CP violation, observed in both

$B^\pm \rightarrow K^\pm \pi^+ \pi^-$ and $B^\pm \rightarrow \pi^\pm \pi^+ \pi^-$ decays around the $\rho(770)$ mass region, can be attributed to the final-state interference between the S-wave and P-wave in the Dalitz plot.

A. CP asymmetry induced by rescattering

Previous publications [7,8] showed evidence for a possible source of CP violation produced by the long-distance strong phase through $\pi^+\pi^- \leftrightarrow K^+K^-$ rescattering. This interaction plays an important role in S-wave $\pi^+\pi^-$ elastic scattering, as was observed by previous experiments [42,43]

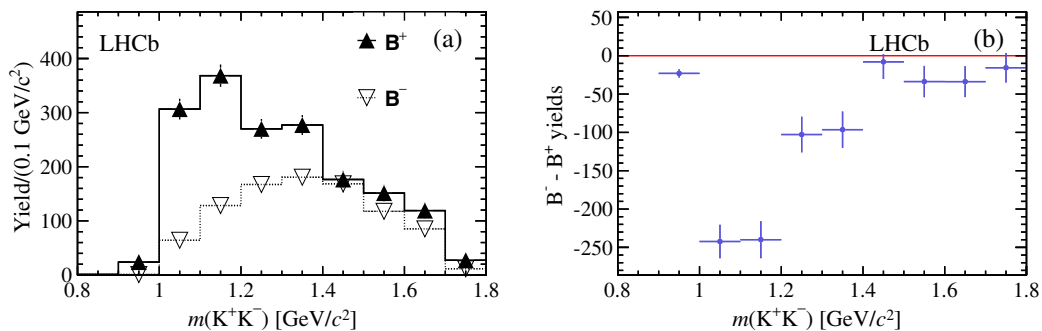


FIG. 7 (color online). Projections in bins of the $m(K^+K^-)$ variable of (a) the number of B^- and B^+ signal events and (b) their difference for $B^\pm \rightarrow \pi^\pm K^+ K^-$ decays. The yields are acceptance-corrected and background-subtracted. A guide line for zero (horizontal red line) was included in plot (b).

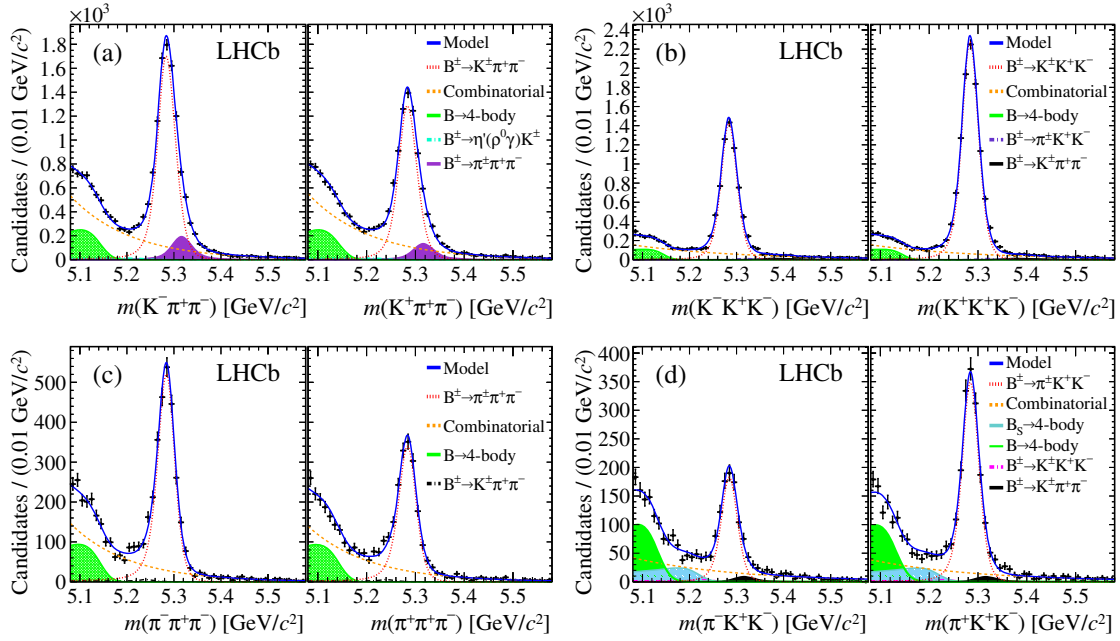


FIG. 8 (color online). Invariant mass distributions in the rescattering regions $[m(\pi^+\pi^-)$ or $m(K^+K^-)$ between 1.0 and 1.5 GeV/c^2] for (a) $B^\pm \rightarrow K^\pm\pi^+\pi^-$, (b) $B^\pm \rightarrow K^\pm K^+K^-$, (c) $B^\pm \rightarrow \pi^\pm\pi^+\pi^-$ and (d) $B^\pm \rightarrow \pi^\pm K^+K^-$ decays. The left panel in each figure shows the B^- candidates and the right panel shows the B^+ candidates.

in the $m(\pi^+\pi^-)$ mass region between 1.0 and 1.5 GeV/c^2 . The CPT symmetry requires that the sum of partial widths of a family of final states related to each other by strong rescattering, such as the four channels analyzed here, are identical for particles and antiparticles. As a consequence, positive CP asymmetry in some channels implies negative CP asymmetry in other channels of the same family.

The large data samples in the present study allow this effect to become evident, as shown in Figs. 4, 5, 6 and 7. Large asymmetries are observed for all the final states in the region between 1.0 and 1.5 GeV/c^2 . Figure 8 shows the invariant mass distributions for events with $m(\pi^+\pi^-)$ and $m(K^+K^-)$ in this interval, excluding the ϕ -meson mass region for the $B^\pm \rightarrow K^\pm K^+K^-$ mode. The measured CP asymmetries corresponding to the figure are given in Table III. Decays involving a K^+K^- pair in the final state have a larger CP asymmetry than their partner channels with a $\pi^+\pi^-$ pair. The asymmetries are positive for channels with a $\pi^+\pi^-$ pair and negative for those with a K^+K^- pair. This indicates that the mechanism of $\pi^+\pi^- \leftrightarrow K^+K^-$ rescattering could play an important role in CP violation in charmless three-body B^\pm decays.

B. CP asymmetry due to interference between partial waves

In hadronic three-body decays, there is another long-distance strong-interaction phase, which stems from the amplitudes of intermediate resonances. The Breit-Wigner propagator associated with an intermediate resonance can provide a phase that varies with the resonance mass. There is also a phase related to final-state interactions, associated

with each intermediate state that contributes to the same final state. In general, the latter phase is considered constant within the phase space. This phase also includes any short-distance strong phase.

These three sources of strong phases are known to give clear signatures in the Dalitz plane [13,14]. The short-distance direct CP violation is proportional to the difference of the magnitude between the positive and negative amplitudes of the resonance, and is therefore proportional to the square of the Breit-Wigner propagator associated with the resonance.

The interference term has two components. One is associated with the real part of the Breit-Wigner propagator and is directly proportional to $(m_R^2 - s)$, where m_R is the central value of the resonance mass and s is the square of the invariant mass of its decay products. The other component is proportional to the product $m_R\Gamma$, where Γ is the width of the resonance. The relative proportion of real and imaginary terms of these interference components

TABLE III. Signal yields and charge asymmetries in the rescattering regions of $m(\pi^+\pi^-)$ or $m(K^+K^-)$ between 1.0 and 1.5 GeV/c^2 . For the charge asymmetries, the first uncertainty is statistical, the second systematic, and the third is due to the CP asymmetry of the $B^\pm \rightarrow J/\psi K^\pm$ reference mode.

| Decay | N_S | A_{CP} |
|---------------------------------------|-----------------|--|
| $B^\pm \rightarrow K^\pm\pi^+\pi^-$ | 15562 ± 165 | $+0.121 \pm 0.012 \pm 0.017 \pm 0.007$ |
| $B^\pm \rightarrow K^\pm K^+K^-$ | 16992 ± 142 | $-0.211 \pm 0.011 \pm 0.004 \pm 0.007$ |
| $B^\pm \rightarrow \pi^\pm\pi^+\pi^-$ | 4329 ± 76 | $+0.172 \pm 0.021 \pm 0.015 \pm 0.007$ |
| $B^\pm \rightarrow \pi^\pm K^+K^-$ | 2500 ± 57 | $-0.328 \pm 0.028 \pm 0.029 \pm 0.007$ |

gives the final-state interaction phase difference between the two amplitudes.

Another feature of the interference term is the characteristic angular distribution. For a decay involving one vector resonance, the interference term is multiplied by $\cos\theta$, which is a linear function of the other Dalitz variable. As the cosine varies from -1 to 1 , the interference term changes sign around the middle of the Dalitz plot. The short-distance CP violation does not change sign because it is proportional to the square of the amplitude ($\cos^2\theta$).

The charge asymmetry in $B^\pm \rightarrow \pi^\pm\pi^+\pi^-$ decays changes sign, as shown in Fig. 4, at a value of $m(\pi^+\pi^-)$ close to the $\rho(770)$ resonance. This is an indication of the dominance of the long-distance interference effect in this region of the Dalitz plot. Moreover, since this change of sign occurs for both $\cos\theta > 0$ and $\cos\theta < 0$, the dominant term of the Dalitz interference is inferred to be the real part of the Breit-Wigner propagator.

When the interference between the P-wave and the S-wave involves two resonances, as for $B^\pm \rightarrow K^\pm\pi^+\pi^-$ decays, with $\rho(770)$ and $f_0(980)$ resonances, the dominant component of the real Dalitz CP asymmetry is proportional to a product of the type $(m_\rho^2 - s)(m_{f_0}^2 - s)$, and thus it has two zeros, as can be seen in Fig. 5. In the $\cos\theta < 0$ region there is a zero around the $\rho(770)$ mass and another one around the $f_0(980)$ meson mass. However, in the region of $\cos\theta > 0$, a clear change of sign is only seen around the $f_0(980)$ mass.

The yield of the $f_0(980)$ resonance in $B^\pm \rightarrow K^\pm\pi^+\pi^-$ decays depends on $\cos\theta$ (Fig. 5). The yield around the $f_0(980)$ mass for $\cos\theta > 0$ is almost twice that of the region with $\cos\theta < 0$. The magnitude of the CP

asymmetry indicates the opposite dependence. Also, the yield around the $\rho(770)$ resonance in the $B^\pm \rightarrow \pi^\pm\pi^+\pi^-$ decay changes significantly in the two $\cos\theta$ regions (Fig. 4). The largest yield in the $\rho(770)$ mass region with a small CP asymmetry occurs for $\cos\theta < 0$, while there is a large CP asymmetry with fewer events in the $\rho(770)$ mass region for $\cos\theta > 0$. One possible explanation is that the fractions of tree and penguin contributions may vary across the phase space [17]. Understanding this effect may be important for performing amplitude analyses.

The CP asymmetry around the $\rho(770)$ peak in the $\pi^+\pi^-$ invariant mass changes sign depending on the invariant mass and angular distribution. To quantify the CP violation in the region where vector particles contribute without losing sensitivity to the interference asymmetry behavior, the region is divided into four sectors. Sectors I and III are on the low-mass side of the resonance mass [$0.47 < m(\pi^+\pi^-)_{\text{low}} < 0.77 \text{ GeV}/c^2$ for $B^\pm \rightarrow \pi^\pm\pi^+\pi^-$ decays], while sectors II and IV are on the high-mass side [$0.77 < m(\pi^+\pi^-)_{\text{low}} < 0.92 \text{ GeV}/c^2$]. Sectors I and II are delimited by $\cos\theta > 0$ (upper part of the Dalitz plot), while sectors III and IV are delimited by $\cos\theta < 0$ (lower part).

Figure 9 shows the invariant mass distributions for $B^\pm \rightarrow \pi^\pm\pi^+\pi^-$ decays divided into these four sectors. The charge asymmetries are measured using the same method as for the inclusive asymmetries. Similar measurements of the CP asymmetries are performed for events restricted to regions dominated by the $\rho(770)$ and $K^*(892)$ resonances in $B^\pm \rightarrow K^\pm\pi^+\pi^-$ decays, and the $\phi(1020)$ resonance in $B^\pm \rightarrow K^\pm K^+K^-$ decays, with the results given in Table IV. Only the decays involving the $\rho(770)$ resonance have a significant CP asymmetry. The $K^*(892)$ charge asymmetry

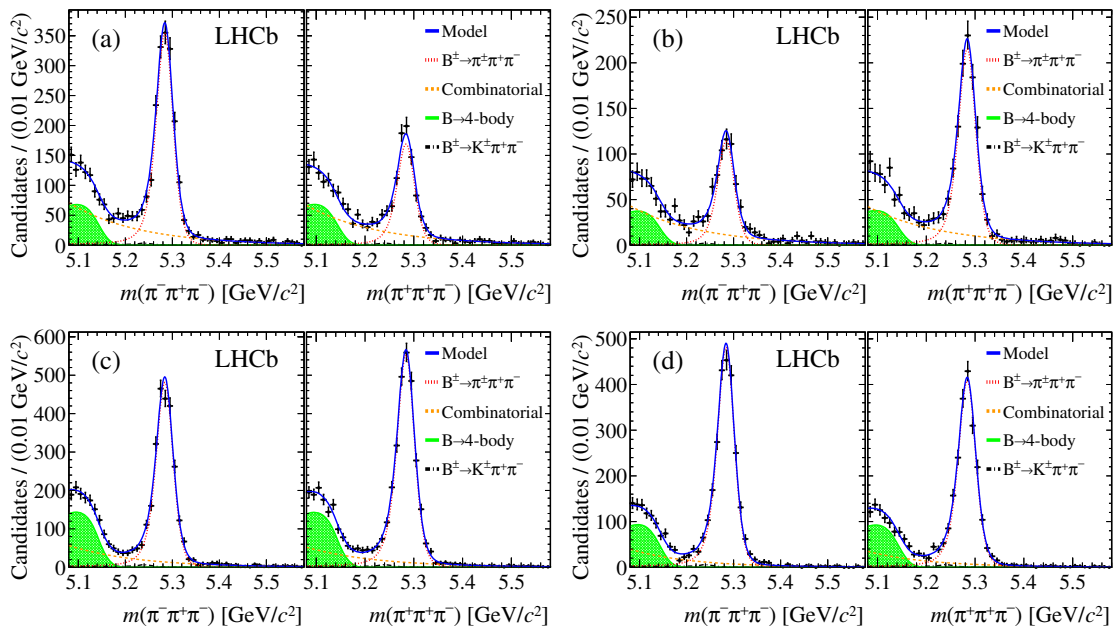


FIG. 9 (color online). Invariant mass distribution of $B^\pm \rightarrow \pi^\pm\pi^+\pi^-$ candidates restricted to (a) sector I, (b) sector II, (c) sector III and (d) sector IV. The left panel in each figure shows the B^- candidates and the right panel shows the B^+ candidates.

TABLE IV. Signal yields and charge asymmetries in the regions dominated by the vector resonances. For the charge asymmetries, the first uncertainty is statistical, the second systematic, and the third is due to the CP asymmetry of the $B^\pm \rightarrow J/\psi K^\pm$ reference mode.

| Decay mode | Resonance | Sector | N_S | A_{CP} |
|---|-----------|--------|-----------------|--|
| $B^\pm \rightarrow K^\pm \pi^+ \pi^-$ | ρ | I | 2909 ± 80 | $-0.052 \pm 0.032 \pm 0.047 \pm 0.007$ |
| | | II | 6136 ± 100 | $+0.140 \pm 0.018 \pm 0.034 \pm 0.007$ |
| | | III | 2856 ± 86 | $+0.598 \pm 0.036 \pm 0.079 \pm 0.007$ |
| | | IV | 2107 ± 55 | $-0.208 \pm 0.043 \pm 0.042 \pm 0.007$ |
| $B^\pm \rightarrow K^\pm \pi^+ \pi^-$ | K^* | I | 11095 ± 115 | $+0.002 \pm 0.013 \pm 0.011 \pm 0.007$ |
| | | II | 7159 ± 89 | $+0.007 \pm 0.016 \pm 0.005 \pm 0.007$ |
| | | III | 2427 ± 65 | $-0.009 \pm 0.031 \pm 0.054 \pm 0.007$ |
| | | IV | 9861 ± 124 | $-0.020 \pm 0.015 \pm 0.010 \pm 0.007$ |
| $B^\pm \rightarrow \pi^\pm \pi^+ \pi^-$ | ρ | I | 2629 ± 59 | $+0.302 \pm 0.026 \pm 0.015 \pm 0.007$ |
| | | II | 1653 ± 46 | $-0.244 \pm 0.034 \pm 0.019 \pm 0.007$ |
| | | III | 5204 ± 79 | $-0.076 \pm 0.019 \pm 0.007 \pm 0.007$ |
| | | IV | 4476 ± 72 | $+0.055 \pm 0.020 \pm 0.013 \pm 0.007$ |
| $B^\pm \rightarrow K^\pm K^+ K^-$ | ϕ | I | 3082 ± 56 | $-0.018 \pm 0.024 \pm 0.008 \pm 0.007$ |
| | | II | 4119 ± 64 | $-0.008 \pm 0.021 \pm 0.004 \pm 0.007$ |
| | | III | 1546 ± 39 | $+0.066 \pm 0.034 \pm 0.010 \pm 0.007$ |
| | | IV | 2719 ± 53 | $+0.015 \pm 0.026 \pm 0.002 \pm 0.007$ |

is consistent with zero, as expected and for the $\phi(1020)$ resonance, the results are in agreement with the previous LHCb analysis [44].

VIII. CONCLUSION

We measured the inclusive CP asymmetries for the four charmless three-body charged decays $B^\pm \rightarrow K^\pm \pi^+ \pi^-$, $B^\pm \rightarrow K^\pm K^+ K^-$, $B^\pm \rightarrow \pi^\pm \pi^+ \pi^-$ and $B^\pm \rightarrow \pi^\pm K^+ K^-$,

$$A_{CP}(B^\pm \rightarrow K^\pm \pi^+ \pi^-) = +0.025 \pm 0.004 \pm 0.004 \pm 0.007,$$

$$A_{CP}(B^\pm \rightarrow K^\pm K^+ K^-) = -0.036 \pm 0.004 \pm 0.002 \pm 0.007,$$

$$A_{CP}(B^\pm \rightarrow \pi^\pm \pi^+ \pi^-) = +0.058 \pm 0.008 \pm 0.009 \pm 0.007,$$

$$A_{CP}(B^\pm \rightarrow \pi^\pm K^+ K^-) = -0.123 \pm 0.017 \pm 0.012 \pm 0.007,$$

where the first uncertainty is statistical, the second systematic, and the third is due to the CP asymmetry of the $B^\pm \rightarrow J/\psi K^\pm$ reference mode, with significances of 2.8σ , 4.3σ , 4.2σ and 5.6σ , respectively. The results, which were obtained from an analysis of data corresponding to an integrated luminosity of 3.0 fb^{-1} , are consistent with and supersede the previous LHCb analyses based on 1.0 fb^{-1} of data [7,8].

The CP asymmetries are not uniformly distributed in the phase space. For each of the channels, we observed a significant CP asymmetry in the $m(K^+ K^-)$ or $m(\pi^+ \pi^-)$ invariant mass region between 1.0 and 1.5 GeV/c^2 . These CP asymmetries are positive for the channels that include two pions in the final state and negative for those that include two kaons. These results are in agreement with those from previous LHCb publications [7,8] and could be due to long-distance $\pi^+ \pi^- \leftrightarrow K^+ K^-$ rescattering [9,10]. A comprehensive study of this phenomenon has to involve the complete set of paired channels, including

the $B^\pm \rightarrow K^\pm \pi^0 \pi^0$ and $B^\pm \rightarrow K^\pm \bar{K}^0 K^0$ decays for the $B^\pm \rightarrow K^\pm \pi^+ \pi^-$ family, and the $B^\pm \rightarrow \pi^\pm \pi^0 \pi^0$ and $B^\pm \rightarrow \pi^\pm \bar{K}^0 K^0$ decays for the $B^\pm \rightarrow \pi^\pm \pi^+ \pi^-$ one. The role of the unpaired hadron in two-body $\pi^+ \pi^- \leftrightarrow K^+ K^-$ rescattering merits further investigation [45].

The CP asymmetry related to the $\rho(770)$ resonance in the $\pi^+ \pi^-$ invariant mass below $1 \text{ GeV}/c^2$ was also reported. The behavior of this asymmetry, which crosses zero around the $\rho(770)$ mass in both $B^\pm \rightarrow K^\pm \pi^+ \pi^-$ and $B^\pm \rightarrow \pi^\pm \pi^+ \pi^-$ modes, indicates a CP asymmetry related to the real part of the long-distance interaction between the S-wave and P-wave contributions to $\pi^+ \pi^-$. Further understanding of the resonance contributions and CP asymmetries in these decays will require amplitude analyses.

ACKNOWLEDGMENTS

We express our gratitude to our colleagues in the CERN accelerator departments for the excellent performance of the LHC. We thank the technical and administrative staff at the LHCb institutes. We acknowledge support from CERN and from the national agencies: CAPES, CNPq, FAPERJ and FINEP (Brazil); NSFC (China); CNRS/IN2P3 (France); BMBF, DFG, HGF and MPG (Germany); SFI (Ireland); INFN (Italy); FOM and NWO (The Netherlands); MNiSW and NCN (Poland); MEN/IFA (Romania); MinES and FANO (Russia); MinECo (Spain); SNSF and SER (Switzerland); NASU (Ukraine); STFC (United Kingdom); NSF (USA). The Tier1 computing centres are supported by IN2P3 (France), KIT and BMBF (Germany), INFN (Italy), NWO and SURF (The Netherlands), PIC (Spain), GridPP (United Kingdom). We are indebted to the communities behind the multiple open source software packages on which we depend. We are also thankful for the computing resources and the access to software research and

development tools provided by Yandex LLC (Russia). Individual groups or members have received support from EPLANET, Marie Skłodowska-Curie Actions and ERC (European Union), Conseil général de Haute-Savoie, Labex

ENIGMASS and OCEVU, Région Auvergne (France), RFBR (Russia), XuntaGal and GENCAT (Spain), Royal Society and Royal Commission for the Exhibition of 1851 (United Kingdom).

-
- [1] M. Kobayashi and T. Maskawa, *Prog. Theor. Phys.* **49**, 652 (1973).
- [2] M. Gavela, P. Hernandez, J. Orloff, and O. Pene, *Mod. Phys. Lett. A* **09**, 795 (1994).
- [3] M. Beneke and M. Neubert, *Nucl. Phys.* **B675**, 333 (2003).
- [4] A. Garmash *et al.* (Belle Collaboration), *Phys. Rev. Lett.* **96**, 251803 (2006).
- [5] B. Aubert *et al.* (BABAR Collaboration), *Phys. Rev. D* **78**, 012004 (2008).
- [6] J.-P. Lees *et al.* (BABAR Collaboration), *Phys. Rev. D* **85**, 112010 (2012).
- [7] R. Aaij *et al.* (LHCb Collaboration), *Phys. Rev. Lett.* **111**, 101801 (2013).
- [8] R. Aaij *et al.* (LHCb Collaboration), *Phys. Rev. Lett.* **112**, 011801 (2014).
- [9] B. Bhattacharya, M. Gronau, and J. L. Rosner, *Phys. Lett. B* **726**, 337 (2013).
- [10] I. Bediaga, O. Lourenço, and T. Frederico, *Phys. Rev. D* **89**, 094013 (2014).
- [11] J.-M. Gérard and W.-S. Hou, *Phys. Rev. D* **43**, 2909 (1991).
- [12] M. Bander, D. Silverman, and A. Soni, *Phys. Rev. Lett.* **43**, 242 (1979).
- [13] I. Bediaga, I. I. Bigi, A. Gomes, G. Guerrer, J. Miranda, and A. C. dos Reis, *Phys. Rev. D* **80**, 096006 (2009).
- [14] I. Bediaga, G. Guerrer, and J. M. de Miranda, *Phys. Rev. D* **76**, 073011 (2007).
- [15] L. Leśniak and P. Żenczykowski, *Phys. Lett. B* **737**, 201 (2014).
- [16] Z.-H. Zhang, X.-H. Guo, and Y.-D. Yang, *Phys. Rev. D* **87**, 076007 (2013).
- [17] H.-Y. Cheng and C.-K. Chua, *Phys. Rev. D* **88**, 114014 (2013).
- [18] D. Xu, G.-N. Li, and X.-G. He, *Int. J. Mod. Phys. A* **29**, 1450011 (2014).
- [19] M. Gronau, *Phys. Lett. B* **727**, 136 (2013).
- [20] A. A. Alves Jr. *et al.* (LHCb Collaboration), *JINST* **3**, S08005 (2008).
- [21] M. Adinolfi *et al.*, *Eur. Phys. J. C* **73**, 2431 (2013).
- [22] A. A. Alves Jr. *et al.*, *JINST* **8**, P02022 (2013).
- [23] R. Aaij *et al.*, *JINST* **8**, P04022 (2013).
- [24] T. Sjöstrand, S. Mrenna, and P. Skands, *J. High Energy Phys.* **05** (2006) 026.
- [25] I. Belyaev *et al.*, in *Nuclear Science Symposium Conference Record (NSS/MIC), 2010 IEEE, Knoxville, TN, 2010* (IEEE, New York, 2010), p. 1155.
- [26] D. J. Lange, *Nucl. Instrum. Methods Phys. Res., Sect. A* **462**, 152 (2001).
- [27] P. Golonka and Z. Was, *Eur. Phys. J. C* **45**, 97 (2006).
- [28] J. Allison *et al.* (GEANT4 Collaboration), *IEEE Trans. Nucl. Sci.* **53**, 270 (2006); S. Agostinelli *et al.* (GEANT4 Collaboration), *Nucl. Instrum. Methods Phys. Res., Sect. A* **506**, 250 (2003).
- [29] M. Clemencic, G. Corti, S. Easo, C. R. Jones, S. Miglioranza, M. Pappagallo, and P. Robbe, *J. Phys. Conf. Ser.* **331**, 032023 (2011).
- [30] J. Beringer *et al.* (Particle Data Group), *Phys. Rev. D* **86**, 010001 (2012), and 2013 partial update for the 2014 edition.
- [31] L. Breiman, J. H. Friedman, R. A. Olshen, and C. J. Stone, *Classification and regression trees* (Wadsworth, Belmont, CA, 1984).
- [32] B. P. Roe, H.-J. Yang, J. Zhu, Y. Liu, I. Stancu, and G. McGregor, *Nucl. Instrum. Methods Phys. Res., Sect. A* **543**, 577 (2005).
- [33] A. Hoecker *et al.*, *Proc. Sci.*, ACAT2007 (2007) 040 [arXiv: physics/0703039].
- [34] F. Archilli *et al.*, *JINST* **8**, P10020 (2013).
- [35] H. Albrecht *et al.* (ARGUS Collaboration), *Phys. Lett. B* **229**, 304 (1989).
- [36] R. Aaij *et al.* (LHCb Collaboration), *Phys. Lett. B* **713**, 186 (2012).
- [37] L. Lyons, D. Gibaut, and P. Clifford, *Nucl. Instrum. Methods Phys. Res., Sect. A* **270**, 110 (1988).
- [38] D. M. Santos and F. Dupertuis, *Nucl. Instrum. Methods Phys. Res., Sect. A* **764**, 150 (2014).
- [39] B. Aubert *et al.* (BABAR Collaboration), *Phys. Rev. D* **79**, 072006 (2009).
- [40] Y. Li, C.-D. Lu, and W. Wang, *Phys. Rev. D* **80**, 014024 (2009).
- [41] M. Pivk and F. R. Le Diberder, *Nucl. Instrum. Methods Phys. Res., Sect. A* **555**, 356 (2005).
- [42] D. Cohen, D. Ayres, R. Diebold, S. Kramer, A. Pawlicki, and A. Wicklund, *Phys. Rev. D* **22**, 2595 (1980).
- [43] A. D. Martin and E. Ozmutlu, *Nucl. Phys.* **B158**, 520 (1979).
- [44] R. Aaij *et al.* (LHCb Collaboration), *Phys. Lett. B* **728**, 85 (2014).
- [45] P. Magalhaes, M. R. Robilotta, K. S. F. F. Guimarães, T. Frederico, W. de Paula, I. Bediaga, A. C. dos Reis, C. M. Maekawa, and G. R. S. Zarnauskas, *Phys. Rev. D* **84**, 094001 (2011).
-

R. Aaij,⁴¹ B. Adeva,³⁷ M. Adinolfi,⁴⁶ A. Affolder,⁵² Z. Ajaltouni,⁵ S. Akar,⁶ J. Albrecht,⁹ F. Alessio,³⁸ M. Alexander,⁵¹ S. Ali,⁴¹ G. Alkhazov,³⁰ P. Alvarez Cartelle,³⁷ A. A. Alves Jr.,^{25,38} S. Amato,² S. Amerio,²² Y. Amhis,⁷ L. An,³ L. Anderlini,^{17,a} J. Anderson,⁴⁰ R. Andreassen,⁵⁷ M. Andreotti,^{16,b} J. E. Andrews,⁵⁸ R. B. Appleby,⁵⁴ O. Aquines Gutierrez,¹⁰ F. Archilli,³⁸ A. Artamonov,³⁵ M. Artuso,⁵⁹ E. Aslanides,⁶ G. Auremma,^{25,c} M. Baalouch,⁵ S. Bachmann,¹¹ J. J. Back,⁴⁸ A. Badalov,³⁶ W. Baldini,¹⁶ R. J. Barlow,⁵⁴ C. Barschel,³⁸ S. Barsuk,⁷ W. Barter,⁴⁷ V. Batozskaya,²⁸ V. Battista,³⁹ A. Bay,³⁹ L. Beaucourt,⁴ J. Beddow,⁵¹ F. Bedeschi,²³ I. Bediaga,¹ S. Belogurov,³¹ K. Belous,³⁵ I. Belyaev,³¹ E. Ben-Haim,⁸ G. Bencivenni,¹⁸ S. Benson,³⁸ J. Benton,⁴⁶ A. Berezhnoy,³² R. Bernet,⁴⁰ M.-O. Bettler,⁴⁷ M. van Beuzekom,⁴¹ A. Bien,¹¹ S. Bifani,⁴⁵ T. Bird,⁵⁴ A. Bizzeti,^{17,d} P. M. Bjørnstad,⁵⁴ T. Blake,⁴⁸ F. Blanc,³⁹ J. Blouw,¹⁰ S. Blusk,⁵⁹ V. Bocci,²⁵ A. Bondar,³⁴ N. Bondar,^{30,38} W. Bonivento,^{15,38} S. Borghi,⁵⁴ A. Borgia,⁵⁹ M. Borsato,⁷ T. J. V. Bowcock,⁵² E. Bowen,⁴⁰ C. Bozzi,¹⁶ T. Brambach,⁹ J. van den Brand,⁴² J. Bressieux,³⁹ D. Brett,⁵⁴ M. Britsch,¹⁰ T. Britton,⁵⁹ J. Brodzicka,⁵⁴ N. H. Brook,⁴⁶ H. Brown,⁵² A. Bursche,⁴⁰ G. Busetto,^{22,e} J. Buytaert,³⁸ S. Cadeddu,¹⁵ R. Calabrese,^{16,b} M. Calvi,^{20,f} M. Calvo Gomez,^{36,g} P. Campana,^{18,38} D. Campora Perez,³⁸ A. Carbone,^{14,h} G. Carboni,^{24,i} R. Cardinale,^{19,38,j} A. Cardini,¹⁵ L. Carson,⁵⁰ K. Carvalho Akiba,² G. Casse,⁵² L. Cassina,²⁰ L. Castillo Garcia,³⁸ M. Cattaneo,³⁸ Ch. Cauet,⁹ R. Cenci,⁵⁸ M. Charles,⁸ Ph. Charpentier,³⁸ M. Chefdeville,⁴ S. Chen,⁵⁴ S.-F. Cheung,⁵⁵ N. Chiapolini,⁴⁰ M. Chrzaszcz,^{40,26} K. Ciba,³⁸ X. Cid Vidal,³⁸ G. Ciezarek,⁵³ P. E. L. Clarke,⁵⁰ M. Clemencic,³⁸ H. V. Cliff,⁴⁷ J. Closier,³⁸ V. Coco,³⁸ J. Cogan,⁶ E. Cogneras,⁵ L. Cojocariu,²⁹ P. Collins,³⁸ A. Comerma-Montells,¹¹ A. Contu,¹⁵ A. Cook,⁴⁶ M. Coombes,⁴⁶ S. Coquereau,⁸ G. Corti,³⁸ M. Corvo,^{16,b} I. Counts,⁵⁶ B. Couturier,³⁸ G. A. Cowan,⁵⁰ D. C. Craik,⁴⁸ M. Cruz Torres,⁶⁰ S. Cunliffe,⁵³ R. Currie,⁵⁰ C. D'Ambrosio,³⁸ J. Dalseno,⁴⁶ P. David,⁸ P. N. Y. David,⁴¹ A. Davis,⁵⁷ K. De Bruyn,⁴¹ S. De Capua,⁵⁴ M. De Cian,¹¹ J. M. De Miranda,¹ L. De Paula,² W. De Silva,⁵⁷ P. De Simone,¹⁸ D. Decamp,⁴ M. Deckenhoff,⁹ L. Del Buono,⁸ N. Déléage,⁴ D. Derkach,⁵⁵ O. Deschamps,⁵ F. Dettori,³⁸ A. Di Canto,³⁸ H. Dijkstra,³⁸ S. Donleavy,⁵² F. Dordei,¹¹ M. Dorigo,³⁹ A. Dosil Suárez,³⁷ D. Dossett,⁴⁸ A. Dovbnya,⁴³ K. Dreimanis,⁵² G. Dujany,⁵⁴ F. Dupertuis,³⁹ P. Durante,³⁸ R. Dzhelyadin,³⁵ A. Dziurda,²⁶ A. Dzyuba,³⁰ S. Easo,^{49,38} U. Egede,⁵³ V. Egorychev,³¹ S. Eidelman,³⁴ S. Eisenhardt,⁵⁰ U. Eitschberger,⁹ R. Ekelhof,⁹ L. Eklund,⁵¹ I. El Rifai,⁵ Ch. Elsasser,⁴⁰ S. Ely,⁵⁹ S. Esen,¹¹ H.-M. Evans,⁴⁷ T. Evans,⁵⁵ A. Falabella,¹⁴ C. Färber,¹¹ C. Farinelli,⁴¹ N. Farley,⁴⁵ S. Farry,⁵² R. Fay,⁵² D. Ferguson,⁵⁰ V. Fernandez Albor,³⁷ F. Ferreira Rodrigues,¹ M. Ferro-Luzzi,³⁸ S. Filippov,³³ M. Fiore,^{16,b} M. Fiorini,^{16,b} M. Firlej,²⁷ C. Fitzpatrick,³⁹ T. Fiutowski,²⁷ M. Fontana,¹⁰ F. Fontanelli,^{19,j} R. Forty,³⁸ O. Francisco,² M. Frank,³⁸ C. Frei,³⁸ M. Frosini,^{17,38,a} J. Fu,^{21,38} E. Furfaro,^{24,i} A. Gallas Torreira,³⁷ D. Galli,^{14,h} S. Gallorini,²² S. Gambetta,^{19,j} M. Gandelman,² P. Gandini,⁵⁹ Y. Gao,³ J. García Pardiñas,³⁷ J. Garofoli,⁵⁹ J. Garra Tico,⁴⁷ L. Garrido,³⁶ C. Gaspar,³⁸ R. Gauld,⁵⁵ L. Gavardi,⁹ G. Gavrilo, ³⁰ A. Geraci,^{21,k} E. Gersabeck,¹¹ M. Gersabeck,⁵⁴ T. Gershon,⁴⁸ Ph. Ghez,⁴ A. Gianelle,²² S. Giani,³⁹ V. Gibson,⁴⁷ L. Giubega,²⁹ V. V. Gligorov,³⁸ C. Göbel,⁶⁰ D. Golubkov,³¹ A. Golutvin,^{53,31,38} A. Gomes,^{1,l} C. Gotti,²⁰ M. Grabalosa Gándara,⁵ R. Graciani Diaz,³⁶ L. A. Granado Cardoso,³⁸ E. Graugés,³⁶ G. Graziani,¹⁷ A. Grecu,²⁹ E. Greening,⁵⁵ S. Gregson,⁴⁷ P. Griffith,⁴⁵ L. Grillo,¹¹ O. Grünberg,⁶² B. Gui,⁵⁹ E. Gushchin,³³ Yu. Guz,^{35,38} T. Gys,³⁸ C. Hadjivasiliou,⁵⁹ G. Haefeli,³⁹ C. Haen,³⁸ S. C. Haines,⁴⁷ S. Hall,⁵³ B. Hamilton,⁵⁸ T. Hampson,⁴⁶ X. Han,¹¹ S. Hansmann-Menzemer,¹¹ N. Harnew,⁵⁵ S. T. Harnew,⁴⁶ J. Harrison,⁵⁴ J. He,³⁸ T. Head,³⁸ V. Heijne,⁴¹ K. Hennessy,⁵² P. Henrard,⁵ L. Henry,⁸ J. A. Hernando Morata,³⁷ E. van Herwijnen,³⁸ M. Heß,⁶² A. Hicheur,¹ D. Hill,⁵⁵ M. Hoballah,⁵ C. Hombach,⁵⁴ W. Hulsbergen,⁴¹ P. Hunt,⁵⁵ N. Hussain,⁵⁵ D. Hutchcroft,⁵² D. Hynds,⁵¹ M. Idzik,²⁷ P. Ilten,⁵⁶ R. Jacobsson,³⁸ A. Jaeger,¹¹ J. Jalocha,⁵⁵ E. Jans,⁴¹ P. Jaton,³⁹ A. Jawahery,⁵⁸ F. Jing,³ M. John,⁵⁵ D. Johnson,⁵⁵ C. R. Jones,⁴⁷ C. Joram,³⁸ B. Jost,³⁸ N. Jurik,⁵⁹ M. Kabbalo,⁹ S. Kandybei,⁴³ W. Kanso,⁶ M. Karacson,³⁸ T. M. Karbach,³⁸ S. Karodia,⁵¹ M. Kelsey,⁵⁹ I. R. Kenyon,⁴⁵ T. Ketel,⁴² B. Khanji,²⁰ C. Khurewathanakul,³⁹ S. Klaver,⁵⁴ K. Klimaszewski,²⁸ O. Kochebina,⁷ M. Kolpin,¹¹ I. Komarov,³⁹ R. F. Koopman,⁴² P. Koppenburg,^{41,38} M. Korolev,³² A. Kozlinskiy,⁴¹ L. Kravchuk,³³ K. Kreplin,¹¹ M. Krepis,⁴⁸ G. Krocker,¹¹ P. Krokovny,³⁴ F. Kruse,⁹ W. Kucewicz,^{26,m} M. Kucharczyk,^{20,26,38,f} V. Kudryavtsev,³⁴ K. Kurek,²⁸ T. Kvaratskheliya,³¹ V. N. La Thi,³⁹ D. Lacarrere,³⁸ G. Lafferty,⁵⁴ A. Lai,¹⁵ D. Lambert,⁵⁰ R. W. Lambert,⁴² G. Lanfranchi,¹⁸ C. Langenbruch,⁴⁸ B. Langhans,³⁸ T. Latham,⁴⁸ C. Lazzeroni,⁴⁵ R. Le Gac,⁶ J. van Leerdam,⁴¹ J.-P. Lees,⁴ R. Lefèvre,⁵ A. Leflat,³² J. Lefrançois,⁷ S. Leo,²³ O. Leroy,⁶ T. Lesiak,²⁶ B. Leverington,¹¹ Y. Li,³ T. Likhomanenko,⁶³ M. Liles,⁵² R. Lindner,³⁸ C. Linn,³⁸ F. Lionetto,⁴⁰ B. Liu,¹⁵ S. Lohn,³⁸ I. Longstaff,⁵¹ J. H. Lopes,² N. Lopez-March,³⁹ P. Lowdon,⁴⁰ H. Lu,³ D. Lucchesi,^{22,e} H. Luo,⁵⁰ A. Lupato,²² E. Luppi,^{16,b} O. Lupton,⁵⁵ F. Machefert,⁷ I. V. Machikhiliyan,³¹ F. Maciuc,²⁹ O. Maev,³⁰ S. Malde,⁵⁵ A. Malinin,⁶³ G. Manca,^{15,n} G. Mancinelli,⁶ A. Mapelli,³⁸ J. Maratas,⁵ J. F. Marchand,⁴ U. Marconi,¹⁴ C. Marin Benito,³⁶ P. Marino,^{23,o} R. Märki,³⁹ J. Marks,¹¹ G. Martellotti,²⁵ A. Martens,⁸ A. Martín Sánchez,⁷ M. Martinelli,³⁹ D. Martinez Santos,⁴² F. Martinez Vidal,⁶⁴

D. Martins Tostes,² A. Massafferri,¹ R. Matev,³⁸ Z. Mathe,³⁸ C. Matteuzzi,²⁰ A. Mazurov,^{16,b} M. McCann,⁵³ J. McCarthy,⁴⁵ A. McNab,⁵⁴ R. McNulty,¹² B. McKelley,⁵² B. Meadows,⁵⁷ F. Meier,⁹ M. Meissner,¹¹ M. Merk,⁴¹ D. A. Milanese,⁸ M.-N. Minard,⁴ N. Moggi,¹⁴ J. Molina Rodriguez,⁶⁰ S. Monteil,⁵ M. Morandin,²² P. Morawski,²⁷ A. Mordà,⁶ M. J. Morello,^{23,o} J. Moron,²⁷ A.-B. Morris,⁵⁰ R. Mountain,⁵⁹ F. Muheim,⁵⁰ K. Müller,⁴⁰ M. Mussini,¹⁴ B. Muster,³⁹ P. Naik,⁴⁶ T. Nakada,³⁹ R. Nandakumar,⁴⁹ I. Nasteva,² M. Needham,⁵⁰ N. Neri,²¹ S. Neubert,³⁸ N. Neufeld,³⁸ M. Neuner,¹¹ A. D. Nguyen,³⁹ T. D. Nguyen,³⁹ C. Nguyen-Mau,^{39,p} M. Nicol,⁷ V. Niess,⁵ R. Niet,⁹ N. Nikitin,³² T. Nikodem,¹¹ A. Novoselov,³⁵ D. P. O'Hanlon,⁴⁸ A. Oblakowska-Mucha,²⁷ V. Obraztsov,³⁵ S. Oggero,⁴¹ S. Ogilvy,⁵¹ O. Okhrimenko,⁴⁴ R. Oldeman,^{15,n} G. Onderwater,⁶⁵ M. Orlandea,²⁹ B. Osorio Rodrigues,¹ J. M. Otalora Goicochea,² P. Owen,⁵³ A. Oyanguren,⁶⁴ B. K. Pal,⁵⁹ A. Palano,^{13,q} F. Palombo,^{21,r} M. Palutan,¹⁸ J. Panman,³⁸ A. Papanestis,^{49,38} M. Pappagallo,⁵¹ L. L. Pappalardo,^{16,b} C. Parkes,⁵⁴ C. J. Parkinson,^{9,45} G. Passaleva,¹⁷ G. D. Patel,⁵² M. Patel,⁵³ C. Patrignani,^{19,j} A. Pazos Alvarez,³⁷ A. Pearce,⁵⁴ A. Pellegrino,⁴¹ M. Pepe Altarelli,³⁸ S. Perazzini,^{14,h} E. Perez Trigo,³⁷ P. Perret,⁵ M. Perrin-Terrin,⁶ L. Pescatore,⁴⁵ E. Pesen,⁶⁶ K. Petridis,⁵³ A. Petrolini,^{19,j} E. Picatoste Olloqui,³⁶ B. Pietrzyk,⁴ T. Pilař,⁴⁸ D. Pinci,²⁵ A. Pistone,¹⁹ S. Playfer,⁵⁰ M. Plo Casasus,³⁷ F. Polci,⁸ A. Poluektov,^{48,34} E. Polycarpo,² A. Popov,³⁵ D. Popov,¹⁰ B. Popovici,²⁹ C. Potterat,² E. Price,⁴⁶ J. Prisciandaro,³⁹ A. Pritchard,⁵² C. Prouve,⁴⁶ V. Pugatch,⁴⁴ A. Puig Navarro,³⁹ G. Punzi,^{23,s} W. Qian,⁴ B. Rachwal,²⁶ J. H. Rademacker,⁴⁶ B. Rakotomiamanana,³⁹ M. Rama,¹⁸ M. S. Rangel,² I. Raniuk,⁴³ N. Rauschmayr,³⁸ G. Raven,⁴² S. Reichert,⁵⁴ M. M. Reid,⁴⁸ A. C. dos Reis,¹ S. Ricciardi,⁴⁹ S. Richards,⁴⁶ M. Rihl,³⁸ K. Rinnert,⁵² V. Rives Molina,³⁶ D. A. Roa Romero,⁵ P. Robbe,⁷ A. B. Rodrigues,¹ E. Rodrigues,⁵⁴ P. Rodriguez Perez,⁵⁴ S. Roiser,³⁸ V. Romanovsky,³⁵ A. Romero Vidal,³⁷ M. Rotondo,²² J. Rouvinet,³⁹ T. Ruf,³⁸ H. Ruiz,³⁶ P. Ruiz Valls,⁶⁴ J. J. Saborido Silva,³⁷ N. Sagidova,³⁰ P. Sail,⁵¹ B. Saitta,^{15,n} V. Salustino Guimaraes,² C. Sanchez Mayordomo,⁶⁴ B. Sanmartin Sedes,³⁷ R. Santacesaria,²⁵ C. Santamarina Rios,³⁷ E. Santovetti,^{24,i} A. Sarti,^{18,t} C. Satriano,^{25,c} A. Satta,²⁴ D. M. Saunders,⁴⁶ M. Savrie,^{16,b} D. Savrina,^{31,32} M. Schiller,⁴² H. Schindler,³⁸ M. Schlupp,⁹ M. Schmelling,¹⁰ B. Schmidt,³⁸ O. Schneider,³⁹ A. Schopper,³⁸ M.-H. Schune,⁷ R. Schwemmer,³⁸ B. Sciascia,¹⁸ A. Sciubba,²⁵ M. Seco,³⁷ A. Semennikov,³¹ I. Sepp,⁵³ N. Serra,⁴⁰ J. Serrano,⁶ L. Sestini,²² P. Seyfert,¹¹ M. Shapkin,³⁵ I. Shapoval,^{16,43,b} Y. Shcheglov,³⁰ T. Shears,⁵² L. Shekhtman,³⁴ V. Shevchenko,⁶³ A. Shires,⁹ R. Silva Coutinho,⁴⁸ G. Simi,²² M. Sirendi,⁴⁷ N. Skidmore,⁴⁶ T. Skwarnicki,⁵⁹ N. A. Smith,⁵² E. Smith,^{55,49} E. Smith,⁵³ J. Smith,⁴⁷ M. Smith,⁵⁴ H. Snoek,⁴¹ M. D. Sokoloff,⁵⁷ F. J. P. Soler,⁵¹ F. Soomro,³⁹ D. Souza,⁴⁶ B. Souza De Paula,² B. Spaan,⁹ A. Sparkes,⁵⁰ P. Spradlin,⁵¹ S. Sridharan,³⁸ F. Stagni,³⁸ M. Stahl,¹¹ S. Stahl,¹¹ O. Steinkamp,⁴⁰ O. Stenyakin,³⁵ S. Stevenson,⁵⁵ S. Stoica,²⁹ S. Stone,⁵⁹ B. Storaci,⁴⁰ S. Stracka,^{23,38} M. Straticiu,²⁹ U. Straumann,⁴⁰ R. Stroili,²² V. K. Subbiah,³⁸ L. Sun,⁵⁷ W. Sutcliffe,⁵³ K. Swientek,²⁷ S. Swientek,⁹ V. Syropoulos,⁴² M. Szczekowski,²⁸ P. Szczypka,^{39,38} D. Szilard,² T. Szumlak,²⁷ S. T'Jampens,⁴ M. Teklishyn,⁷ G. Tellarini,^{16,b} F. Teubert,³⁸ C. Thomas,⁵⁵ E. Thomas,³⁸ J. van Tilburg,⁴¹ V. Tisserand,⁴ M. Tobin,³⁹ S. Tolk,⁴² L. Tomassetti,^{16,b} D. Tonelli,³⁸ S. Topp-Joergensen,⁵⁵ N. Torr,⁵⁵ E. Tournefier,⁴ S. Tourneur,³⁹ M. T. Tran,³⁹ M. Tresch,⁴⁰ A. Tsaregorodtsev,⁶ P. Tsopelas,⁴¹ N. Tuning,⁴¹ M. Ubeda Garcia,³⁸ A. Ukleja,²⁸ A. Ustyuzhanin,⁶³ U. Uwer,¹¹ V. Vagnoni,¹⁴ G. Valenti,¹⁴ A. Vallier,⁷ R. Vazquez Gomez,¹⁸ P. Vazquez Regueiro,³⁷ C. Vázquez Sierra,³⁷ S. Vecchi,¹⁶ J. J. Velthuis,⁴⁶ M. Veltri,^{17,u} G. Veneziano,³⁹ M. Vesterinen,¹¹ B. Viaud,⁷ D. Vieira,² M. Vieites Diaz,³⁷ X. Vilasis-Cardona,^{36,g} A. Vollhardt,⁴⁰ D. Volyanskyy,¹⁰ D. Voong,⁴⁶ A. Vorobyev,³⁰ V. Vorobyev,³⁴ C. Voß,⁶² H. Voss,¹⁰ J. A. de Vries,⁴¹ R. Waldi,⁶² C. Wallace,⁴⁸ R. Wallace,¹² J. Walsh,²³ S. Wandernoth,¹¹ J. Wang,⁵⁹ D. R. Ward,⁴⁷ N. K. Watson,⁴⁵ D. Websdale,⁵³ M. Whitehead,⁴⁸ J. Wicht,³⁸ D. Wiedner,¹¹ G. Wilkinson,⁵⁵ M. P. Williams,⁴⁵ M. Williams,⁵⁶ F. F. Wilson,⁴⁹ J. Wimberley,⁵⁸ J. Wishahi,⁹ W. Wislicki,²⁸ M. Witek,²⁶ G. Wormser,⁷ S. A. Wotton,⁴⁷ S. Wright,⁴⁷ S. Wu,³ K. Wyllie,³⁸ Y. Xie,⁶¹ Z. Xing,⁵⁹ Z. Xu,³⁹ Z. Yang,³ X. Yuan,³ O. Yushchenko,³⁵ M. Zangoli,¹⁴ M. Zavertyaev,^{10,v} L. Zhang,⁵⁹ W. C. Zhang,¹² Y. Zhang,³ A. Zhelezov,¹¹ A. Zhokhov,³¹ L. Zhong,³ and A. Zvyagin³⁸

(LHCb Collaboration)

¹Centro Brasileiro de Pesquisas Físicas (CBPF), Rio de Janeiro, Brazil²Universidade Federal do Rio de Janeiro (UFRJ), Rio de Janeiro, Brazil³Center for High Energy Physics, Tsinghua University, Beijing, China⁴LAPP, Université de Savoie, CNRS/IN2P3, Annecy-Le-Vieux, France⁵Clermont Université, Université Blaise Pascal, CNRS/IN2P3, LPC, Clermont-Ferrand, France⁶CPPM, Aix-Marseille Université, CNRS/IN2P3, Marseille, France⁷LAL, Université Paris-Sud, CNRS/IN2P3, Orsay, France⁸LPNHE, Université Pierre et Marie Curie, Université Paris Diderot, CNRS/IN2P3, Paris, France

- ⁹*Fakultät Physik, Technische Universität Dortmund, Dortmund, Germany*
- ¹⁰*Max-Planck-Institut für Kernphysik (MPIK), Heidelberg, Germany*
- ¹¹*Physikalisches Institut, Ruprecht-Karls-Universität Heidelberg, Heidelberg, Germany*
- ¹²*School of Physics, University College Dublin, Dublin, Ireland*
- ¹³*Sezione INFN di Bari, Bari, Italy*
- ¹⁴*Sezione INFN di Bologna, Bologna, Italy*
- ¹⁵*Sezione INFN di Cagliari, Cagliari, Italy*
- ¹⁶*Sezione INFN di Ferrara, Ferrara, Italy*
- ¹⁷*Sezione INFN di Firenze, Firenze, Italy*
- ¹⁸*Laboratori Nazionali dell'INFN di Frascati, Frascati, Italy*
- ¹⁹*Sezione INFN di Genova, Genova, Italy*
- ²⁰*Sezione INFN di Milano Bicocca, Milano, Italy*
- ²¹*Sezione INFN di Milano, Milano, Italy*
- ²²*Sezione INFN di Padova, Padova, Italy*
- ²³*Sezione INFN di Pisa, Pisa, Italy*
- ²⁴*Sezione INFN di Roma Tor Vergata, Roma, Italy*
- ²⁵*Sezione INFN di Roma La Sapienza, Roma, Italy*
- ²⁶*Henryk Niewodniczanski Institute of Nuclear Physics Polish Academy of Sciences, Kraków, Poland*
- ²⁷*AGH - University of Science and Technology, Faculty of Physics and Applied Computer Science, Kraków, Poland*
- ²⁸*National Center for Nuclear Research (NCBJ), Warsaw, Poland*
- ²⁹*Horia Hulubei National Institute of Physics and Nuclear Engineering, Bucharest-Magurele, Romania*
- ³⁰*Petersburg Nuclear Physics Institute (PNPI), Gatchina, Russia*
- ³¹*Institute of Theoretical and Experimental Physics (ITEP), Moscow, Russia*
- ³²*Institute of Nuclear Physics, Moscow State University (SINP MSU), Moscow, Russia*
- ³³*Institute for Nuclear Research of the Russian Academy of Sciences (INR RAN), Moscow, Russia*
- ³⁴*Budker Institute of Nuclear Physics (SB RAS) and Novosibirsk State University, Novosibirsk, Russia*
- ³⁵*Institute for High Energy Physics (IHEP), Protvino, Russia*
- ³⁶*Universitat de Barcelona, Barcelona, Spain*
- ³⁷*Universidad de Santiago de Compostela, Santiago de Compostela, Spain*
- ³⁸*European Organization for Nuclear Research (CERN), Geneva, Switzerland*
- ³⁹*Ecole Polytechnique Fédérale de Lausanne (EPFL), Lausanne, Switzerland*
- ⁴⁰*Physik-Institut, Universität Zürich, Zürich, Switzerland*
- ⁴¹*Nikhef National Institute for Subatomic Physics, Amsterdam, The Netherlands*
- ⁴²*Nikhef National Institute for Subatomic Physics and VU University Amsterdam, Amsterdam, The Netherlands*
- ⁴³*NSC Kharkiv Institute of Physics and Technology (NSC KIPT), Kharkiv, Ukraine*
- ⁴⁴*Institute for Nuclear Research of the National Academy of Sciences (KINR), Kyiv, Ukraine*
- ⁴⁵*University of Birmingham, Birmingham, United Kingdom*
- ⁴⁶*H.H. Wills Physics Laboratory, University of Bristol, Bristol, United Kingdom*
- ⁴⁷*Cavendish Laboratory, University of Cambridge, Cambridge, United Kingdom*
- ⁴⁸*Department of Physics, University of Warwick, Coventry, United Kingdom*
- ⁴⁹*STFC Rutherford Appleton Laboratory, Didcot, United Kingdom*
- ⁵⁰*School of Physics and Astronomy, University of Edinburgh, Edinburgh, United Kingdom*
- ⁵¹*School of Physics and Astronomy, University of Glasgow, Glasgow, United Kingdom*
- ⁵²*Oliver Lodge Laboratory, University of Liverpool, Liverpool, United Kingdom*
- ⁵³*Imperial College London, London, United Kingdom*
- ⁵⁴*School of Physics and Astronomy, University of Manchester, Manchester, United Kingdom*
- ⁵⁵*Department of Physics, University of Oxford, Oxford, United Kingdom*
- ⁵⁶*Massachusetts Institute of Technology, Cambridge, Massachusetts 02139, USA*
- ⁵⁷*University of Cincinnati, Cincinnati, Ohio 45221, USA*
- ⁵⁸*University of Maryland, College Park, Maryland 20742, USA*
- ⁵⁹*Syracuse University, Syracuse, New York 13244, USA*
- ⁶⁰*Pontifícia Universidade Católica do Rio de Janeiro (PUC-Rio), Rio de Janeiro, Brazil (associated with Institution Universidade Federal do Rio de Janeiro (UFRJ), Rio de Janeiro, Brazil)*
- ⁶¹*Institute of Particle Physics, Central China Normal University, Wuhan, Hubei, China (associated with Institution Center for High Energy Physics, Tsinghua University, Beijing, China)*
- ⁶²*Institut für Physik, Universität Rostock, Rostock, Germany (associated with Institution Physikalisches Institut, Ruprecht-Karls-Universität Heidelberg, Heidelberg, Germany)*

- ⁶³*National Research Centre Kurchatov Institute, Moscow, Russia (associated with Institution Institute of Theoretical and Experimental Physics (ITEP), Moscow, Russia)*
- ⁶⁴*Instituto de Física Corpuscular (IFIC), Universitat de Valencia-CSIC, Valencia, Spain (associated with Institution Universitat de Barcelona, Barcelona, Spain)*
- ⁶⁵*KVI - University of Groningen, Groningen, The Netherlands (associated with Institution Nikhef National Institute for Subatomic Physics, Amsterdam, The Netherlands)*
- ⁶⁶*Celal Bayar University, Manisa, Turkey (associated with Institution European Organization for Nuclear Research (CERN), Geneva, Switzerland)*

^aAlso at Università di Firenze, Firenze, Italy.

^bAlso at Università di Ferrara, Ferrara, Italy.

^cAlso at Università della Basilicata, Potenza, Italy.

^dAlso at Università di Modena e Reggio Emilia, Modena, Italy.

^eAlso at Università di Padova, Padova, Italy.

^fAlso at Università di Milano Bicocca, Milano, Italy.

^gAlso at LIFAELS, La Salle, Universitat Ramon Llull, Barcelona, Spain.

^hAlso at Università di Bologna, Bologna, Italy.

ⁱAlso at Università di Roma Tor Vergata, Roma, Italy.

^jAlso at Università di Genova, Genova, Italy.

^kAlso at Politecnico di Milano, Milano, Italy.

^lAlso at Universidade Federal do Triângulo Mineiro (UFTM), Uberaba-MG, Brazil.

^mAlso at AGH - University of Science and Technology, Faculty of Computer Science, Electronics and Telecommunications, Kraków, Poland.

ⁿAlso at Università di Cagliari, Cagliari, Italy.

^oAlso at Scuola Normale Superiore, Pisa, Italy.

^pAlso at Hanoi University of Science, Hanoi, Viet Nam.

^qAlso at Università di Bari, Bari, Italy.

^rAlso at Università degli Studi di Milano, Milano, Italy.

^sAlso at Università di Pisa, Pisa, Italy.

^tAlso at Università di Roma La Sapienza, Roma, Italy.

^uAlso at Università di Urbino, Urbino, Italy.

^vAlso at P.N. Lebedev Physical Institute, Russian Academy of Science (LPI RAS), Moscow, Russia.